

- Université Paris VI
- RuG, University of Groningen

Numerical simulation of bloodflow through straight stenotic vessels

Bram de Bruin

December 13, 2000

- P-Y. Lagrée (LMM/UPMC)
- A. E. P. Veldman (RuG)

Contents

1	Introduction	4
2	Modeling	5
2.1	Mathematical model	5
2.2	Numerical model	6
2.3	Reduced Navier-Stokes	8
2.4	Thwaites Method	9
3	Numerical Simulation of 2D flows	10
3.1	A simple unsteady example	10
3.2	An unsteady pulsatile example	12
3.3	A comparison with Thwaites' method	14
3.4	Realistic dimensions	16
3.4.1	Example with constant inflow	18
3.4.2	Example with pulsatile inflow	19
3.5	Steady flow in an aneurysm	19
3.6	Non-axisymmetrical stenosis	21
3.7	Stenotic bifurcation	23
3.8	Conclusions	24
4	The BIACORE 2000	25
4.1	The flow simulation through the BIACORE 2000	26
4.2	Discussion	27
5	Three dimensional stenosis flow	29
5.1	'One direction' stenosis	29
5.2	Axisymmetrical stenosis	31
6	Conclusions	36
A	Womersley analysis	37
A.1	The direct Womersley solution	37
A.1.1	Plots of U_{wom}	38
A.1.2	Putting α large in the solution	39

A.2	Asymptotical point of view α large	39
A.2.1	Perfect fluid	39
A.2.2	Boundary layer	40
A.3	Remarks	40
A.3.1	The wall shear stress	40
A.4	Small α	41
A.4.1	Analytical solution for small α	41
A.4.2	Asymptotic solution for small α	41
B	Explanatory vocabulary	42
	Bibliography	43

Chapter 1

Introduction

During the months september, october, november and december of the year 2000 I have done a traineeship at the University of Pierre et Marie Curie in Paris. The background of the traineeship is how to simulate blood flow through arteries. This could be very useful in the future in hospitals. For example, specialists could predict if a certain shape of an artery could cause a stenosis and do something about it before people really get the stenosis.

At the university in Paris a code has been developed by P-Y Lagr e and Lorthois [10] and Koen Goorman [7] for liquid, incompressible flow through tubes, using the Reduced Navier-Stokes equations. In this method the Navier-Stokes equations are simplified using the boundary layer theory. This results in the Reduced Navier-Stokes equations which are more simple to solve numerically than the full Navier-Stokes equations. However they still are approximations.

The RuG, the University of Groningen, has developed during the last years a code, see D.J. Kort [8] and E. Loots [12], which solves the complete Navier-Stokes equations in very much different cases. For example, almost all geometries can be used and there is the possibility for in- and outflow cells as well as liquid sloshing in a cube. With this code blood flow can also be simulated by making the right geometry and use in- and outflow cells. Although this code does not make real approximations it might not be very useful in the near future because it takes much more time to solve the full Navier-Stokes equations.

Further, these two different methods will be called RNS, Reduced Navier-Stokes, and NS, Navier-Stokes. The goal of this traineeship is to compare these two codes in different cases. Also some practical problems are simulated.

In chapter 2 the mathematical model as well as the three used numerical models are explained in four sections. In chapter 3 a lot of simulations are done for straight 2D tubes with or without stenoses in case of a constant inflow velocity or a pulsatile one. Chapter 4 is all about the BIACORE 2000, a machine in the hospital that simulates blood flow and measures quantities of chemical reactions at the wall. Finally, in chapter 5 simulations are made for the more realistic 3D geometries with stenoses. Chapter 6 contains the overall conclusions.

Chapter 2

Modeling

In this chapter we first explain the mathematical model of liquid flow with his boundary conditions that are necessary in the of blood flow through tubes. After that, in section 2.2, 2.3 and 2.4, the three used numerical models are explained.

2.1 Mathematical model

Blood flow through arteries of course is a 3D flow. So the 3D Navier Stokes equations hold. However a straight blood vessel is in first approximation a cylinder. So a axi symmetrical form of these equations could be used. In the examples of section 3 a 2D code is used to solve the equations. The results can be interpreted as the mechanics in the crosssection of the artery. For any 2D flow domain filled with a Newtonian fluid (like blood in first approximations) the unsteady incompressible Navier-Stokes equations hold. These equations are given here below.

- First we have the equation expressing the conservation of mass in each volume:

$$\frac{\partial u}{\partial x} + \frac{\partial v}{\partial y} = 0$$

Here u denotes the velocity in the x -direction and v the velocity in the y -direction.

- Second we have the equations expressing the conservation of momentum in x -, and y -direction, respectively:

$$\begin{aligned} \frac{\partial u}{\partial t} + u \frac{\partial u}{\partial x} + v \frac{\partial u}{\partial y} &= -\frac{\partial p}{\partial x} + \nu \left(\frac{\partial^2 u}{\partial x^2} + \frac{\partial^2 u}{\partial y^2} \right) + F_x \\ \frac{\partial v}{\partial t} + u \frac{\partial v}{\partial x} + v \frac{\partial v}{\partial y} &= -\frac{\partial p}{\partial y} + \nu \left(\frac{\partial^2 v}{\partial x^2} + \frac{\partial^2 v}{\partial y^2} \right) + F_y \end{aligned}$$

In these equations, t denotes the time, p the pressure scaled by the density, ν the kinematic viscosity and $\mathbf{F} = (F_x, F_y)^T$ the external body force. Our simulation does not include an external body force. Therefore it will be omitted here.

With $\mathbf{u} = (u, v)^T$ these equations can also be denoted as:

$$\nabla \cdot \mathbf{u} = 0 \quad (2.1)$$

$$\frac{\partial \mathbf{u}}{\partial t} + (\mathbf{u} \cdot \nabla) \mathbf{u} = -\nabla p + \nu(\nabla \cdot \nabla) \mathbf{u} \quad (2.2)$$

Of course these equations need boundary conditions. The blood cannot flow through the wall and due to its viscosity it sticks to the wall. This yields at the wall:

$$u = 0 \quad \text{and} \quad v = 0$$

The pulsatile flow of the blood is simulated at the inlet of the artery by pushing it in. The blood volume to be pushed in, can be controlled by the area of the inflow cross section and the blood velocity at the inlet. Therefore we have the inflow condition:

$$\mathbf{u}(x, y, t) = \mathbf{u}_{in}(t)$$

At the outlet we prescribe the fluid to be unidirectional and the pressure to be equal to the pressure outside of the fluid :

$$\frac{\partial \mathbf{u}}{\partial n} = 0 \quad \text{and} \quad p = p_0$$

Here $\mathbf{n} = (n_x, n_y)$ is the outward pointing normal on the outflow boundary.

Other conditions on the inflow and outflow are also possible. The inflow could be described fully developed and at the outlet the condition $-p\mathbf{n} + \frac{1}{Re} \frac{\partial \mathbf{u}}{\partial n} = 0$ could be imposed. However, the conditions imposed have been proved very useful in other simulations and are already implemented.

On the other hand these conditions cause to need an extra long tube. The developing of the flow in the direction of the wall needs time and length. At the start of the simulated artery, it has to be fully developed and not only a function of time. The outflow also has a small effect on the flow near the end of the tube causing to need for an extra bit of tube at the end of the simulated artery.

2.2 Numerical model

For the computations of the blood flow the computational domain is decomposed into five different kind of cells: boundary cells, exterior cells, inflow cells and outflow cells. The exterior cells play no role in the discretization process, so they will not be mentioned here again.

The grid used is totally staggered. All the velocities are placed in the middle of the lateral faces of the cells and the pressures are placed in the centres of the cells. Now the Navier- Stokes equations have to be discretized. The projection method is used here. This is an explicit method using the abbreviation:

$$\mathbf{R}^n = -\nabla(\mathbf{u}^n \mathbf{u}^{nT}) + \nu \nabla \cdot \nabla \mathbf{u}^n$$

Now we split equation 2.2, the conservation of momentum, into two pieces using u^* and discretize them in time using forward Euler:

$$\begin{aligned}\frac{\mathbf{u}^* - \mathbf{u}^n}{\delta t} &= \mathbf{R}^n \\ \frac{\mathbf{u}^{n+1} - \mathbf{u}^*}{\delta t} &= -\nabla p^{n+1}\end{aligned}$$

When we add these two equations, the u^* vanishes and the result are the time discretized Navier-Stokes equations: (Together with the equation of mass of course)

$$\frac{\mathbf{u}^{n+1} - \mathbf{u}^n}{\delta t} = \mathbf{R}^n - \nabla p^{n+1} \quad (2.3)$$

$$\nabla \cdot \mathbf{u}^{n+1} = 0 \quad (2.4)$$

Here δt is the time step and n and $n + 1$ denote the old and the new time level.

We have to discretize in space too. Because we can not use any boundary condition yet, this discretization can only be made for flow cells. First the discrete versions of the divergence and the gradient operators have to be defined. The divergence operator ∇ becomes D_h and the gradient operator grad becomes G_h . In both cases h denotes the spatial step. Because we only discretize in flow cells, this has to be expressed in the divergence operator as well: $D_h = D_h^F + D_h^B$. The F represents here the inner flow domain and the B the boundary. Because of the unknown boundary velocities the complete discretization becomes

$$\begin{aligned}D_h^F \mathbf{u}^{n+1} + D_h^B \mathbf{u}^{n+1} &= 0 \\ \mathbf{u}^{n+1} &= \mathbf{u}^n + \delta t \mathbf{R}_h^n - \delta t G_h p^{n+1}\end{aligned}$$

By substitution of the second into the first equation, the pressure Poisson equation is obtained:

$$D_h^F G_h p^{n+1} = D_h^F \left(\frac{\mathbf{u}^n}{\delta t} + \mathbf{R}_h^n \right) + D_h^B \frac{\mathbf{u}^n}{\delta t} \quad (2.5)$$

This equation is solved, with the SOR method, and we can obtain the velocity field by substituting the pressure in equation 2.3.

Finally we have to look at the boundary. In boundary cells the pressure is not defined, so we can not use the Navier-Stokes equations. Therefore the velocities at the boundary are set to satisfy $\mathbf{u} = 0$ at the wall. This is done by interpolation and the use of mirror points.

This method is stable if:

$$\text{CFL} = \frac{U_{max} \delta t}{h} < 1 \quad \text{and} \quad \nu \frac{\delta t}{\delta x^2} < \frac{1}{2}$$

2.3 Reduced Navier-Stokes

Because this report involves the comparison of a full Navier-Stokes code and a Reduced Navier-stokes code, the ideas of the Reduced Navier-Stokes equations will be explained here.

To derive the RNS equations from the NS equations first the variable will be made dimensionless. The x , y , u , v , t and p will be scaled using parameters from the system. For the y we use the height of the tube so that the dimensionless variable will range from 0 to 1. For the u , which is the velocity in x -direction we use a scale of the input velocity U_0 . So this results in:

$$x = L\bar{x}, \quad y = H\bar{y}, \quad u = U_0\bar{u}, \quad v = V\bar{v}, \quad p = P\bar{p}, \quad t = T\bar{t}$$

Here variable with a bar denotes the dimensionless variables. The other scales will be derived later.

After substituting these new variables into the conservation of mass we can conclude that we have to choose $\frac{U_0}{L} = \frac{V}{H}$. After substituting these variables in the momentum equations and stating that the viscous forces must be of the same strength as the convective forces, we see that $\frac{\nu U_0}{H^2} = \frac{U_0^2}{L}$. This leads to the scale for x :

$$L = \frac{U_0 H^2}{\nu} = H Re_H$$

Because we only consider $Re_H \gg 1$ the scale for x is much larger than the scale for y and thus the $\frac{\partial^2 u}{\partial x^2}$ vanishes from the equation of momentum. Also $\frac{\partial p}{\partial y} = 0$ because $U_0 \gg V$. For the scale of the pressure we choose $P = \rho U_0^2$ and for $T = \frac{L}{U_0}$.

When all this is applied to the Navier stokes equations and they are rewritten the following equations remain, called the Reduced Navier Stokes equations:

$$\frac{\partial u}{\partial x} + \frac{\partial v}{\partial y} = 0 \tag{2.6}$$

$$\frac{\partial u}{\partial t} + u \frac{\partial u}{\partial x} + v \frac{\partial u}{\partial y} = -\frac{\partial p}{\partial x} + \frac{\partial^2 u}{\partial y^2} \tag{2.7}$$

$$\frac{\partial p}{\partial y} = 0 \tag{2.8}$$

At the wall we use the same boundary conditions that are used in the Navier Stokes code:

$$u = v = 0$$

At the entrance we have a fixed pressure and the velocity is given:

$$u(x = 0, y, t) = u_{in}(t) \quad \text{and} \quad p = 0$$

These equations are being solved by a code using a finite difference method. In our examples, unless otherwise noted, U_0 will be 1 and the Reynolds number (Re_H) will be 100. An analytic solution using this idea is given in Appendix A.

2.4 Thwaites Method

In this section a short explanation of the Thwaites method will be given, see also Comolet [6], Schlichting [15] and Veldman [17]. This method is derived from an integral form of the stationary Boundary Layer equations called the 'Von Kármán' equation:

$$\frac{\partial \delta_2}{\partial x} + \frac{\delta_2(2+H)}{U} \frac{\partial U}{\partial x} = \frac{C_f}{2}$$

where $H = \frac{\delta_1}{\delta_2}$ and C_f the wall shear stress coefficient. The δ_1 and δ_2 are abbreviations for:

$$\begin{aligned} \delta_1 &= \int_0^\infty \left(1 - \frac{u}{U}\right) dy \\ \delta_2 &= \int_0^\infty \frac{u}{U} \left(1 - \frac{u}{U}\right) dy \end{aligned}$$

In the boundary layer the assumption is made that the u varies from 0 at the wall to U at the border of the boundary layer and the outer fluid which flows with velocity U . So $u = Uf\left(\frac{y}{\delta}\right)$ in the boundary layer. The equations can be rewritten now using

$$Y = \frac{\delta_2^2}{\nu}, \quad T = \frac{\nu \tau_0 \delta_2}{\rho U}, \quad \lambda = -\frac{\delta_2^2}{\nu} \frac{dU}{dx}$$

to:

$$UY' = 2T - 2\lambda(H + 2)$$

Because T and H are both function of λ we can rewrite the equation as:

$$Y' = \frac{F(\lambda)}{U} \tag{2.9}$$

It happens to be that $F(\lambda)$ is nearly a linear function of λ . The second equation that is solved is the equation of flux conservation, i.e. the product of the velocity in the outer fluid and the width of that outer region remains constant. So this results in:

$$U(h_1 - 2\delta_1) = cst \tag{2.10}$$

In the used code the equations 2.9 and 2.10 are solved. In 2.10 the constant is chosen equal to 1.

Chapter 3

Numerical Simulation of 2D flows

In this chapter we first look at an simple example of flow through a straight artery without stenosis. After that we will simulate a stenotic artery with pulsatile inflow. In section 3.3 a comparison is made with the Thwaites' method of C. Villain. After that we take again the first stenotic example but with realistic dimensions! In section 3.5 simulation of flow through an aneurysm, which is the inverse of an stenosis, is made. Section 3.6 discusses the non-axisymmetric stenoses and 3.7 an bifurcation with or without stenosis.

3.1 A simple unsteady example

The first simple example we used was not realistic in the case of an artery of a human being, but it was more to validate the codes. There are two stationary parallel planes at height h and $-h$. In our example we used $h = 1\text{cm}$. We used the inflow condition: $u = 1\frac{\text{cm}}{\text{s}}$ and $v = 0$ at the entrance. It is known that this inflow condition will result, after a long enough length of the planes and a long enough time, in a streamprofile that can analytically be described by the (2D-)Poiseuille flow. The velocity between the plates is then given by

$$u(y) = \frac{1}{2\mu} \frac{dp}{dx} (y^2 - h^2) \quad (3.1)$$

Here μ denotes the dynamic viscosity. Note that this equation denotes a parabolic velocity profile. In figure 3.1 the velocity in the middle of the tube, i.e. $y = 0$, is plotted against the length of the tube at four different times. Notice that it takes time to fully develop the Poiseuille flow. After about 20 seconds, this profile does not change anymore and the flow is fully Poiseuille at 10 cm from the beginning. The same is plotted in figure 3.2 but this is a combined plot with the NS results as well as the RNS results. The RNS method is quite faster then the NS method: RNS calculates this fluid with 800 points in x-direction and 500 points in y-direction, that

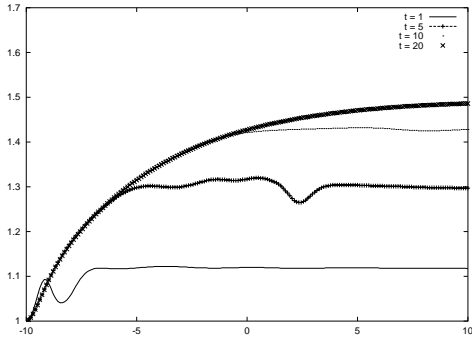


Figure 3.1: At different times, the velocity in the middle of the tube, i.e. $y = 0$, is plotted against the length of the tube for the Navier Stokes code. ($Re=100$) x in cm

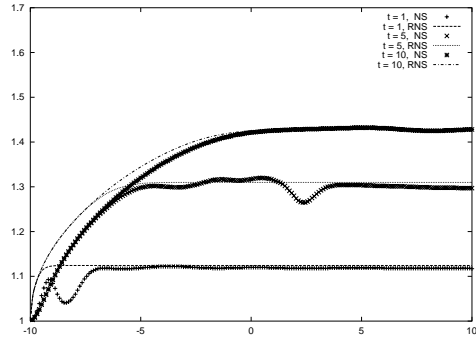


Figure 3.2: At different times, the velocity in the middle of the artery, i.e. $y = 0$, is plotted against the length of the tube. For the NS and the RNS code. The scales for the x and t here is $x_{NS} = 100x_{RNS} + 5$ and $t_{NS} = 100t_{RNS}$. ($Re=100$) x in cm

makes 400.000 points, in approximately 50 minutes. The NS method uses a grid of 200 by 50 points, so only 10.000 points, but calculates about 12 minutes. In the first steps of the calculation Comflo takes a lot time to iterate the pressure but after the stationary flow profile is achieved it goes quite quick because Comflo iterates until a certain precision is achieved. Anyhow, the RNS is visible a lot quicker than NS if you take into account that RNS uses 40 times as much points!

In figure 3.3 the pressure is plotted in the middle of the tube from the NS results,

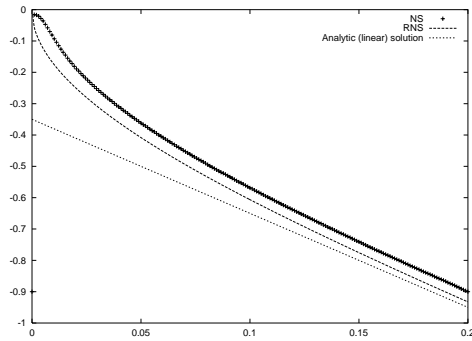


Figure 3.3: Comparison of the pressure as a function of the length of the tube at $y = 0$. ($Re=100$)

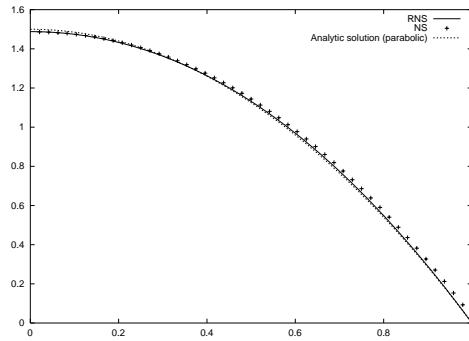


Figure 3.4: Velocity from the middle of the tube to the wall at the end of the tube. ($Re=100$)

the RNS results as well as the analytically solution which is derived from the $\frac{dp}{dx}$ in

the Poiseuille stream profile. The volume flow can be written as follows

$$Q = \int_{-h}^h u(y)dy = \frac{1}{2\mu} \frac{dp}{dx} \frac{2}{3} h^3$$

and must be equal to $U_0 * 2h$. This leads to the following expression for $\frac{dp}{dx}$:

$$\frac{dp}{dx} = \frac{6\mu U_0}{h^2}$$

In figure 3.4 the velocity as function of the y at the end of the tube is plotted. Here are also the NS, the RNS and the analytical solution plotted. From the picture it is obvious that both methods almost have the same parabolic profile as the analytical solution 3.1.

These four examples were made with $Re_h = 100$. In figure 3.5 the final velocities as function of the tube length are plotted again for different Reynolds numbers as well as the dimensionless RNS result. We observe that when the Reynolds number increases, the NS method tends to RNS.

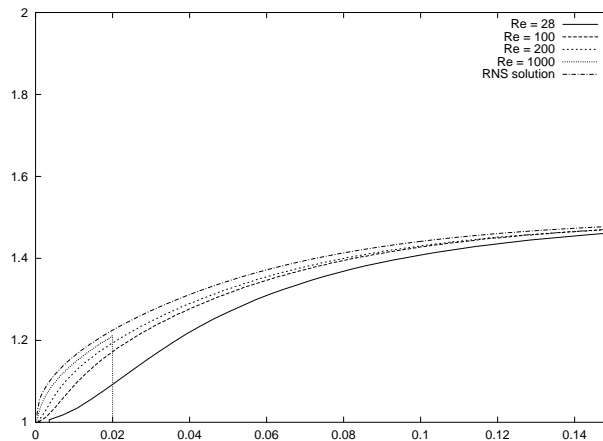


Figure 3.5: The stationary velocities at the middle of the tube, i.e. $y = 0$ are plotted against the length of the tube for different Reynolds numbers. The longitudinal scale used here is the RNS scale. (dimensionless)

3.2 An unsteady pulsatile example

In this section the first of the unsteady examples in a artery with a stenosis will be discussed. Here as in all examples the artery is still a stiff tube. This stenosis has the shape of a cosinus that 'lies' on the wall, so its minimum in the lower wall is at the height of the wall as is its maximum at the higher wall. This is shown in figure 3.6. Of course the height and the length of the stenosis can be changed manually.

The stenosis used in the picture is twice as high as the one used in the example to make its shape better visible.

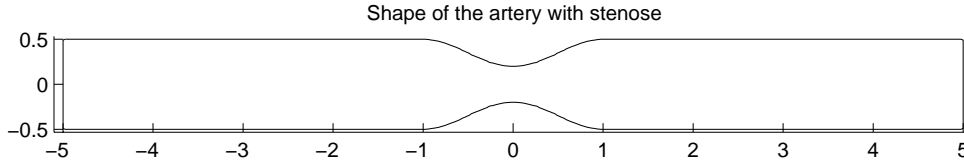


Figure 3.6: Artery with a stenosis twice as large as used.

We used an instationairy inflow condition:

$$u(x, y, t) = 0.25 \cos(t) + 0.75$$

This inflow condition is independent of x and y but only of t . The maximum value, at $t = k * 2\pi, k \in \mathbb{N}$, is 1 and the minimum value at $t = \pi + k * 2\pi, k \in \mathbb{N}$ is 0.5. This can be seen in figures 3.7, 3.8, 3.9 and 3.10 where the velocity in the

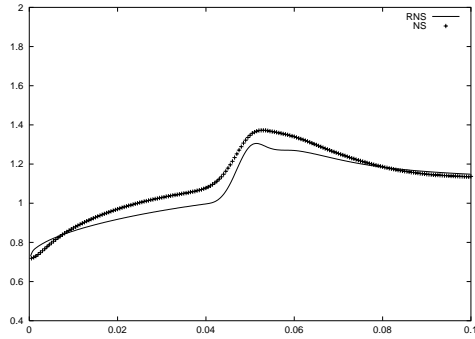


Figure 3.7: The velocity in the middle at $t = \frac{5\pi}{2}$. Dimensionless scales.

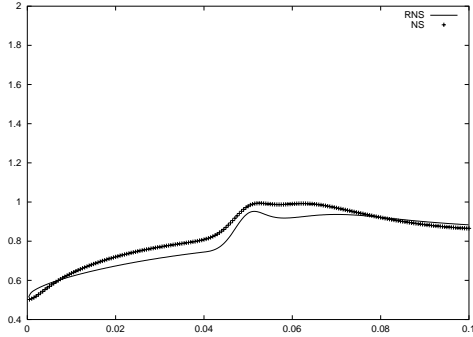


Figure 3.8: The velocity in the middle at $t = 3\pi$. Dimensionless scales.

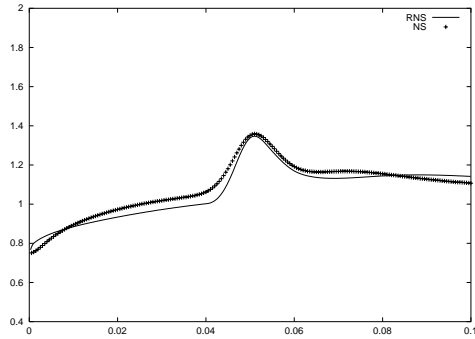


Figure 3.9: The velocity in the middle at $t = \frac{7\pi}{2}$. Dimensionless scales.

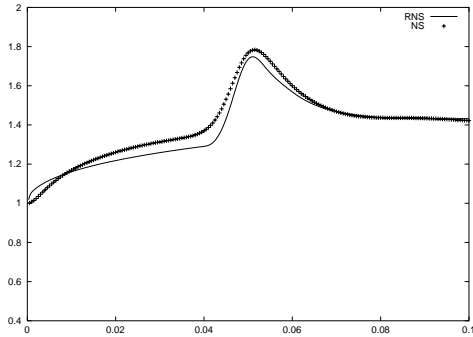


Figure 3.10: The velocity in the middle at $t = 4\pi$. Dimensionless scales.

middle of the tube is plotted against the length of the tube at four different times: $t = \frac{5\pi}{2}$, $t = 3\pi$, $t = \frac{7\pi}{2}$ and $t = 4\pi$ respectively. So these are the times average value with negative slope, the minimum value, the average value with positive slope and the maximum value respectively. It can be seen that these value for the velocity occur at the beginning of the tube, but because the inflow is independent y , the velocity in the middle of the tube immediately increases as a result of the boundary condition at the walls. This was already seen in figure 3.1.

It is clear that the velocities of the two methods almost agree in all pictures. This is not the case for the pressure which can be seen in figures 3.11, 3.12, 3.13 and 3.14.

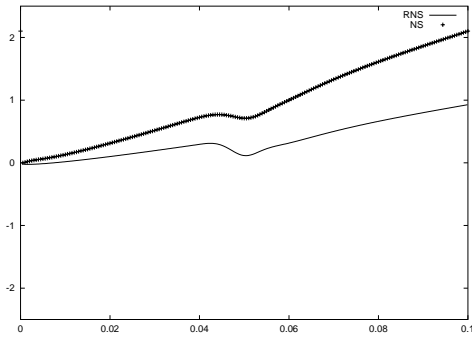


Figure 3.11: The pressure in the middle at $t = \frac{5\pi}{2}$. Dimensionless scales.

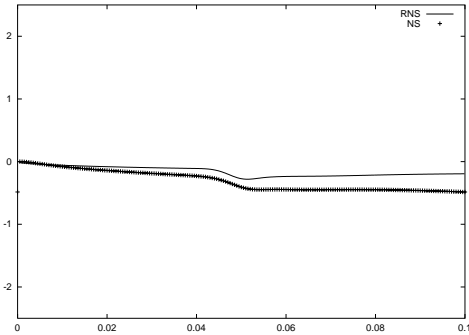


Figure 3.12: The pressure in the middle at $t = 3\pi$. Dimensionless scales.

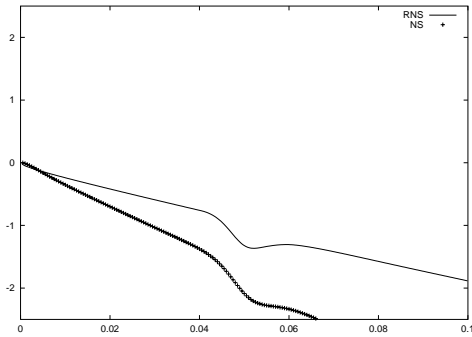


Figure 3.13: The pressure in the middle at $t = \frac{7\pi}{2}$. Dimensionless scales.

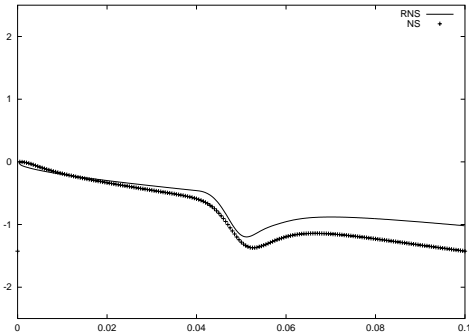


Figure 3.14: The pressure in the middle at $t = 4\pi$. Dimensionless scales.

3.3 A comparison with Thwaites' method

In this section the comparison between NS, RNS and Thwaites method is discussed, see 2.4. C. Villain made a code that solves the Boundary Layer equations using Thwaites' method. There is another geometry used, shown in figure 3.15.

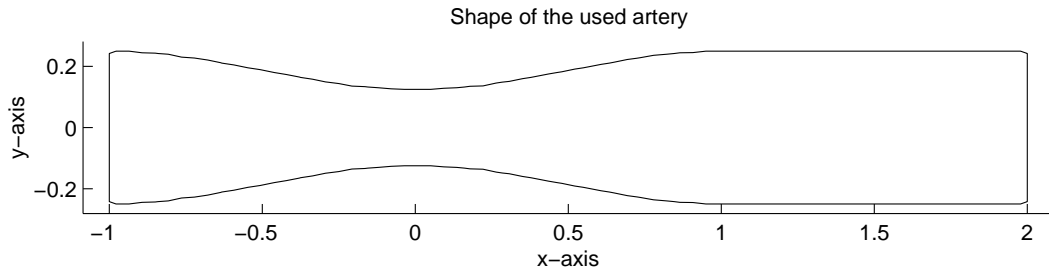


Figure 3.15: The used geometry.(dimensions in *cm*)

There are two simulations used. First we simulated a constant inflow with inflow velocity $u = 350 \frac{cm}{s}$. The results can be seen in figure 3.16.

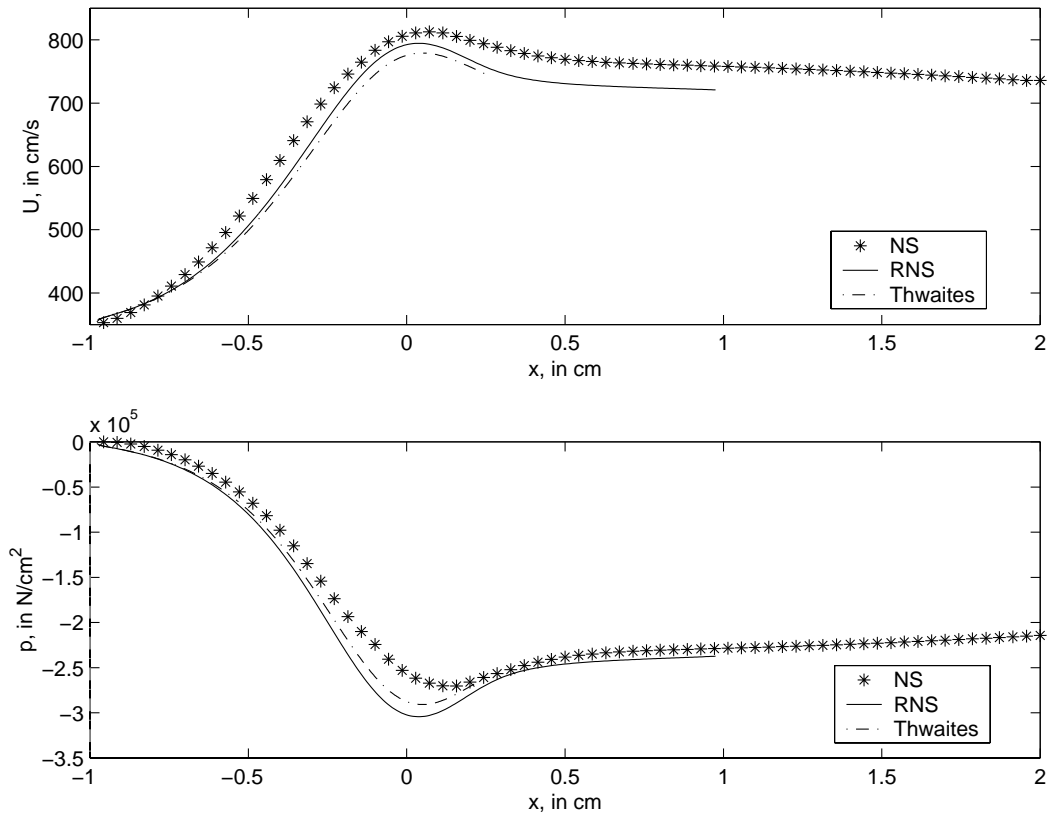


Figure 3.16: The velocity on top and the pressure at the bottom for the three methods. ($Re=583$)

Because $h = 0.5 \text{ cm}$ and $\nu = 0.152 \frac{\text{cm}^2}{\text{s}}$ In this plot, as well as in the plot for unsteady inflow, the Thwaites code stops far before the stenosis is ended because it can not go further than the separation point. After this the method does not work well any more because the U is prescribed instead of δ_1 . In figure 3.17 and 3.18 we used an

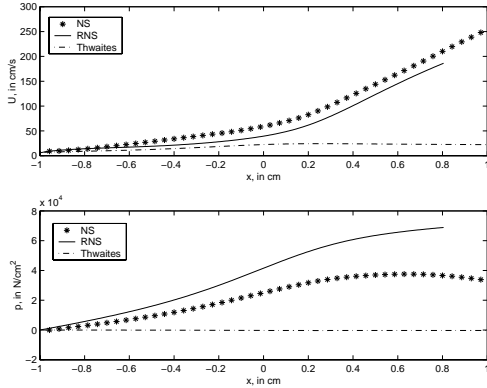


Figure 3.17: The velocity on top and the pressure at the bottom for the three methods at minimal inflow velocity. (Re=583)

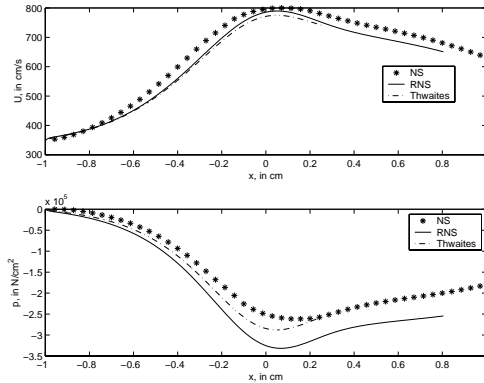


Figure 3.18: The velocity on top and the pressure at the bottom for the three methods at maximal inflow velocity. (Re=583)

unsteady inflow of the form:

$$u_{in} = 350 \frac{\cos(100\pi t) + 1}{2}$$

To improve the NS computation we have to increase the tube to avoid negative effects of the outflow boundary conditions. This because the outflow condition of the NS method is a bit different from the others. The frequency is chosen to be very small because in this case it is sure that even the NS method will give fast results.

3.4 Realistic dimensions

From Siegel [16], some realistic data of how a blood vessel looks like and what kind of stenoses are possible in it were used. The stenosis pictured in figure 3.6 is of the same form as the writers of the article used to approximate a real stenosis. However, the actual values of the distances are different. They looked at short and long stenoses, respectively with length of 6 and 12 times the radius of the artery. For both stenoses they studied 50, 75 and 90% stenosis. So that is more than in example 3.2, where $\frac{0.15}{0.5} = 30\%$ stenosis is used. The artery in this case is also much narrower, the radius is only 0.2 cm., and the inflow much larger. They used an inflow of $100 \frac{\text{ml}}{\text{min}}$.

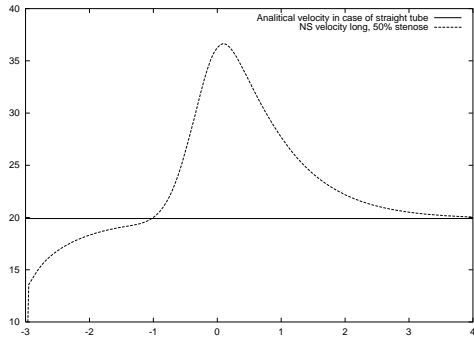


Figure 3.19: The velocity in the middle in case of a long stenosis. x in cm .

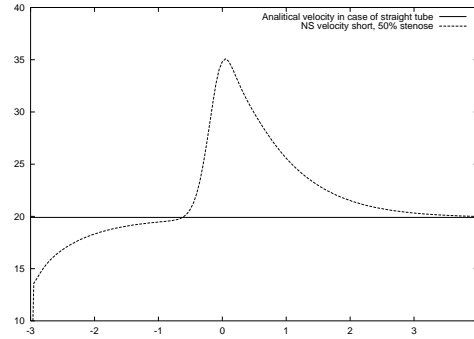


Figure 3.20: The velocity in the middle in case of a short stenosis. x in cm .

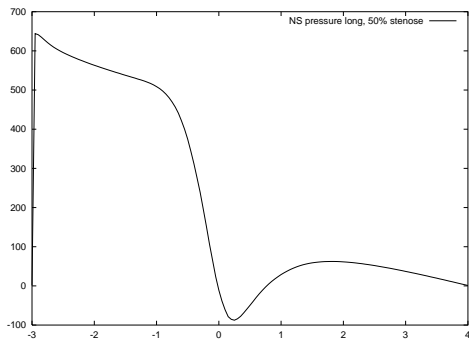


Figure 3.21: The pressure in the middle in case of a long stenosis. x in cm .

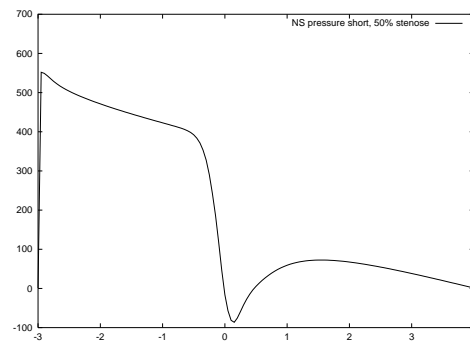


Figure 3.22: The pressure in the middle in case of a short stenosis. x in cm .

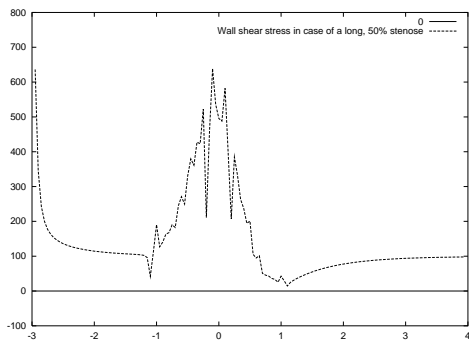


Figure 3.23: The wall shear stress at the lower boundary in case of a long stenosis. Note the bad representation as a result of the discretization. x in cm .

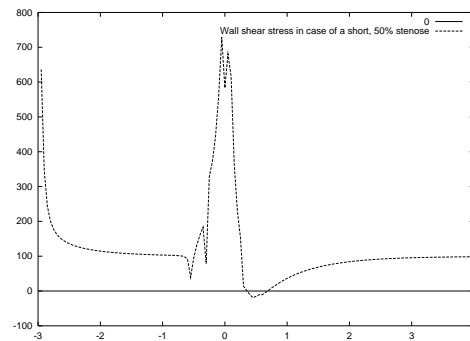


Figure 3.24: The wall shear stress at the lower boundary in case of a short stenosis. Note the bad representation as a result of the discretization. x in cm .

3.4.1 Example with constant inflow

First we simulate this by using the constant inflow velocity of $100 \frac{ml}{min}$. In this case that corresponds with $u_{in} = \frac{100/60}{0.2^2 \pi} \approx 13.269 \frac{cm}{sec}$. So $Re_h = 75$.

In the figures 3.19 and 3.20 the velocity and in figures 3.21 and 3.22 the pressure are plotted at the middle of the artery. The first plot is of a long stenosis and the second of a short stenosis. In both cases the stenoses centers are at $x = 0$ and a 50% stenosis is used.

Further there are also made two plots of the wall shear stress (figures 3.23 and 3.24) in order to compare them with the plots made by the author. The shear stresses at to lower are written into a file. Actually, for each x , $\frac{du}{dy}$ at the wall is written in this file.

Comflo first checks whether a cell is a boundary cell or not and if it is neighbour 'above' him is a fluid cell. In this case he calculates the quotient of the velocity just above the boundary and the cell width in y-direction. If the boundary lies just in a corner of the cell, then the $\frac{du}{dy}$ will be greater then if the boundary will be almost in the middle of the cell. That is why the plot is not very smooth in the area of the bump.

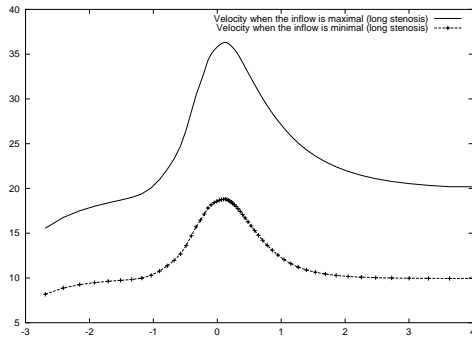


Figure 3.25: The velocity in the middle in case of a long stenosis. x in cm .

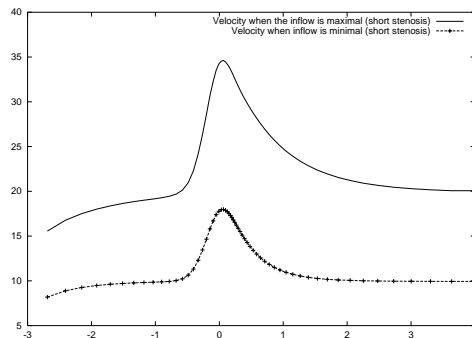


Figure 3.26: The velocity in the middle in case of a short stenosis. x in cm .

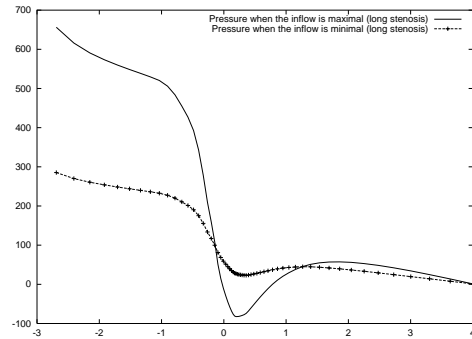


Figure 3.27: The pressure in the middle in case of a long stenosis. x in cm .

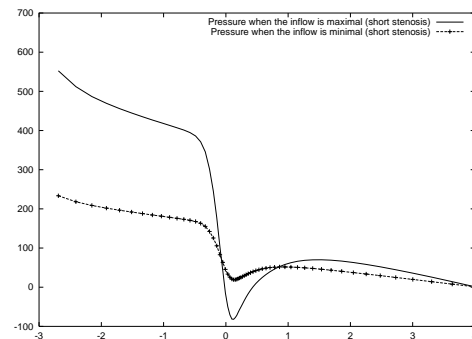


Figure 3.28: The pressure in the middle in case of a short stenosis. x in cm .

Especially in the case of the long stenosis this does not work very good. This because more cells had to be used in order to solve the problem. Some of the cells there get an horizontal boundary in the area of the stenosis and other a line with a small derivate.

It is visible in case of the short stenosis that at the end of the stenosis the wall shear stress is negative. This means that the velocity near the wall is pointed in the other direction as would be expected. In the figure of the long stenosis this is not visible, mainly because of the fact that the data for this figure were not very good.

3.4.2 Example with pulsatile inflow

In this case we used again a cosinus-inflow. This time to better approximate the realistic data, it is multiplied by the u_{in} of the last section. So our new inflow-function is:

$$u_{in}(t) = 13.269 * (0.25 * \cos(t) + 0.75)$$

So again $Re_h = 75$. The same results as in the previous section are plotted. So we have the velocities in figures 3.25 and 3.26 and the pressure in figures 3.27 and 3.28 when the inflow speed is maximal and minimal.

3.5 Steady flow in an aneurysm

So a stenosis is a little narrow section of an artery as shown in figure 3.6. The opposite of a stenosis is an aneurysm: The diameter will be more than 150% of the diameter you expect in the artery. Like is shown in figure 3.29.

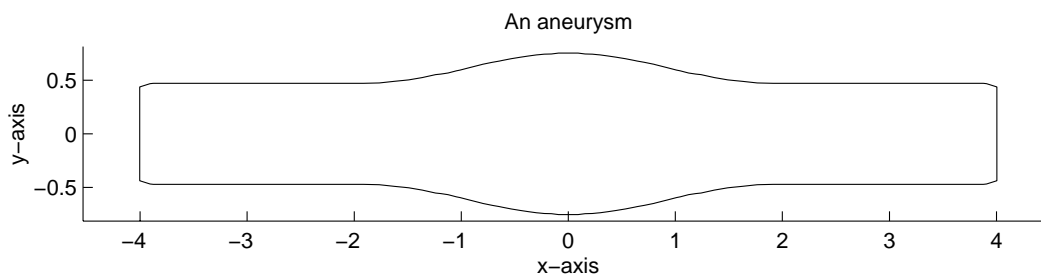


Figure 3.29: An artery with an aneurysm. x and y in cm .

These aneurysms are also very dangerous. For example if an aneurysm in the aorta ruptures, which might happen, the patient has 10 % change of surviving mainly because he can not get to the hospital in time.

The dimensions that were used are realistic dimensions for an aneurysm in the aorta. They were taken from Bluestein and al.[3]. Two different Poiseuille inflow velocities

are used with different volume flow yielding a Reynolds number of 900 and 3600. In figures 3.30 and 3.31 the stream lines through the aneurysm for these two different cases are plotted. It is clearly visible that in the aneurysm itself is a great area of backward flow.

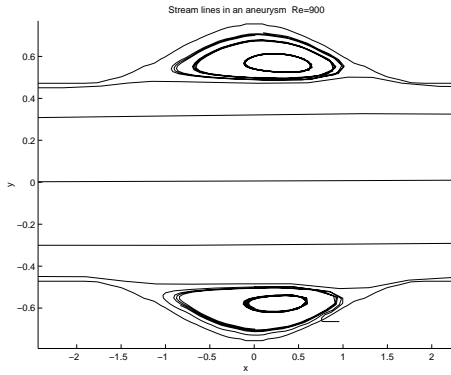


Figure 3.30: The stream lines through the aneurysm with Reynolds number equal to 900. Dimensions in *cm*

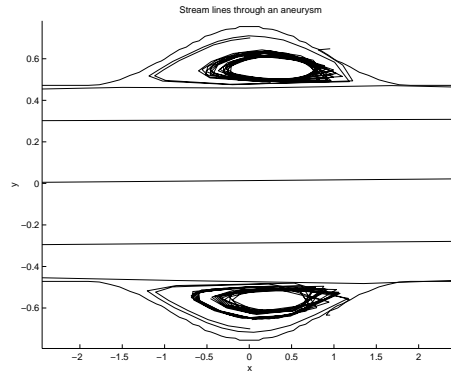


Figure 3.31: The stream lines through the aneurysm with Reynolds number equal to 3600. Dimensions in *cm*

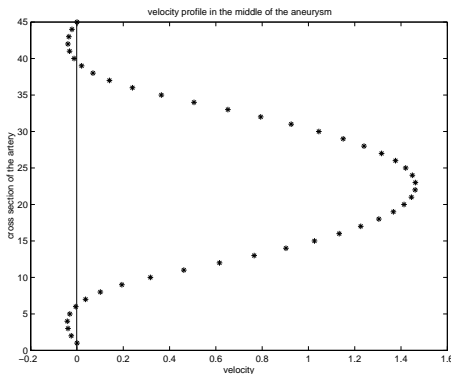


Figure 3.32: Velocity profile at $x = 0$, i.e. in the middle of the aneurysm. $Re = 900$. Dimensions in *cm*

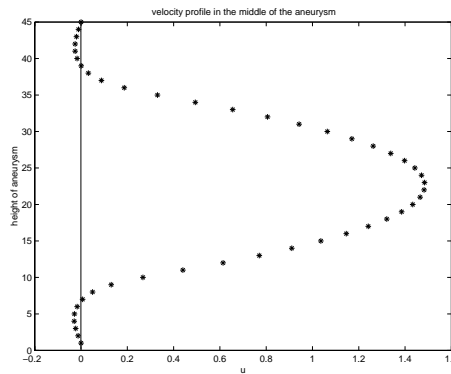


Figure 3.33: Velocity profile at $x = 0$, i.e. in the middle of the aneurysm. $Re = 3600$. Dimensions in *cm*

In figures 3.32 and 3.33 the velocities in the middle of the aneurysm is plotted against the height of it. Here again it is for $Re = 900$ as well as $Re = 3600$ very good visible that a backward flow occurs.

3.6 Non-axisymmetrical stenosis

Here we will look at stenoses that are the same in shape at the upper and the lower wall, but one part is shifted in x-direction as is shown in figure 3.34.

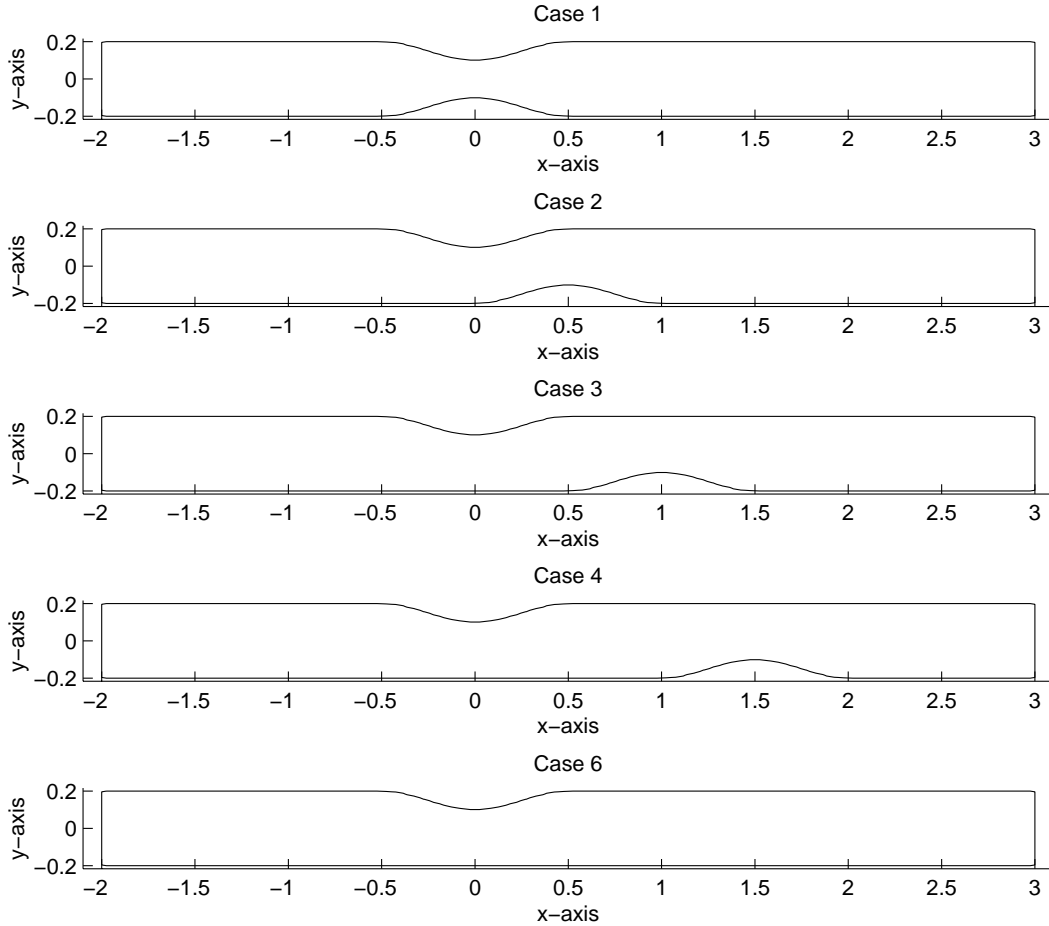


Figure 3.34: The five stenoses that were used in this simulation. Dimensions in cm

The purpose of this section is to verify if the idea is right that when if the stenosis is split in two parts of which the second is placed further upstream than the first, the upstream part will have no influence on the flow further downstream.

Following this idea in the case 3, the flow for $x < 0.5$ should remain the same as in case 6.

We used in this simulation everywhere a flat inflow velocity of $40 \frac{cm}{s}$, which gives us a $Re_h \approx 200$. In figure 3.35 the velocity in the middle of the tube is plotted against the length of it. Note that not the whole tube is represented in the figure but only the part that we are interested in. The velocity is given for the fluid through stenosis 1,2,3,4 and 6. Notice that there is no difference between stenosis 3 and reference

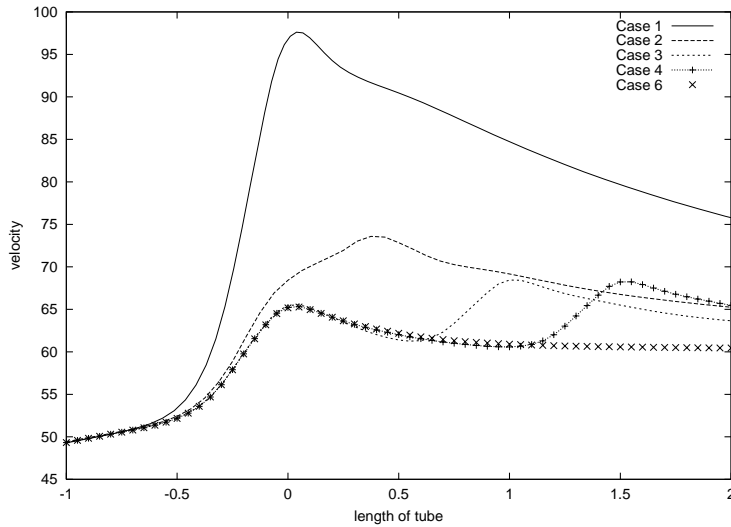


Figure 3.35: The velocity in the middle of the tube for stenosis 1, 2, 3, 4 and 6. Dimensions in *cm*

stenosis 6 for $x < 0.5$, so the idea is right: there is no influence of the downstream bump on the upstream one.

These results were also compared with the results of the RNS method. In figure 3.36 the velocity in the middle of the tube for both methods is given in case of a 'normal' stenosis 1. In figure 3.37 the same velocity is given for the stenoses 2, 3 and 6 from Comflo and for the RNS method with stenosis 6. Note the different scale of the velocities! As expected there is almost no difference between the velocities in 3.35 for the cases 3,4 and 6. At least for cases 4 and 6. In figure 3.37 the difference

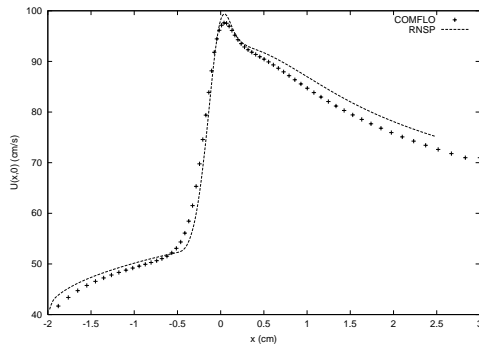


Figure 3.36: The velocity in the middle of the tube for stenosis 1, both Comflo and RNS

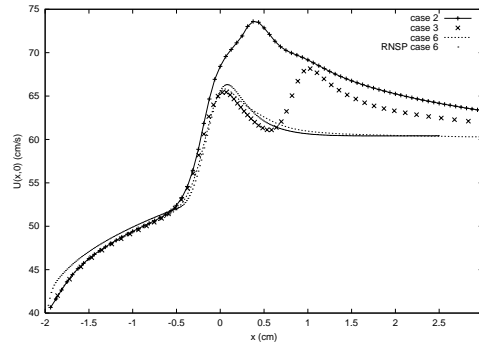


Figure 3.37: The velocity in the middle of the tube for stenosis 2, 3 and 6 for Comflo and RNS (only shape 6)

between case 3 and case 6 for $x < 0.5$ is clearly visible, instead of in figure 3.35. This can be explained by two reasons. First the scale of the y-axis in figure 3.37

has a range of 35 while the range in figure 3.35 is 55. So in figure 3.37 a difference is more easily visible. Second the simulations in figure 3.35 are all made with a grid of 100X50 points while in figure 3.37 for some simulations a 80X40 stretched grid is used! Notice the different distance of the points for cases 2 and 3.

3.7 Stenotic bifurcation

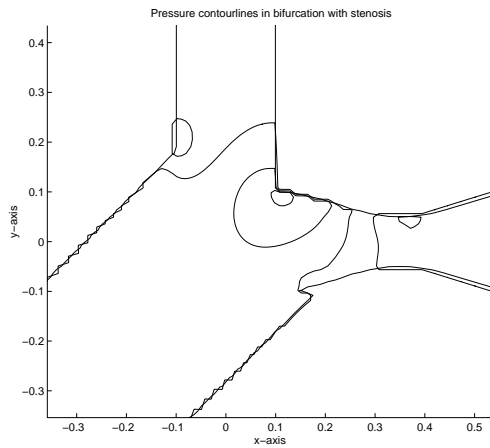


Figure 3.38: Pressure contour lines a stenotic bifurcation. Dimensions in *cm*

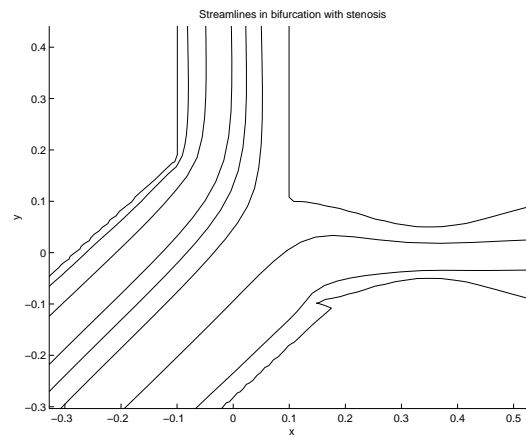


Figure 3.39: The stream lines through a stenotic bifurcation. Dimensions in *cm*

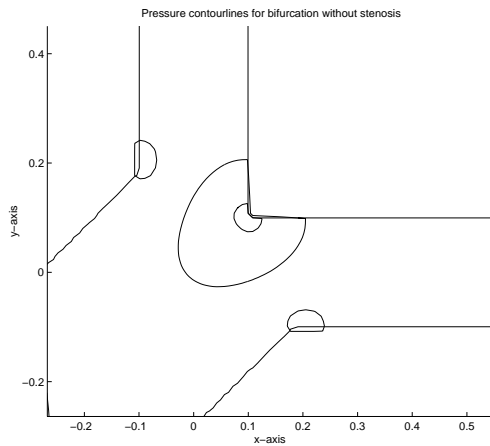


Figure 3.40: Pressure contour lines a non-stenotic bifurcation. Dimensions in *cm*

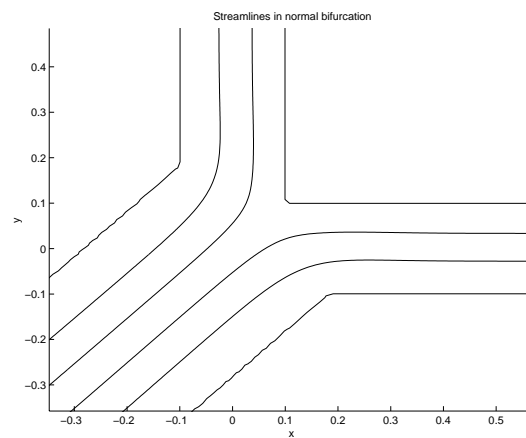


Figure 3.41: The stream lines through a non-stenotic bifurcation. Dimensions in *cm*

In this section a start is made for a next investigation which will mainly cover blood flow through bifurcations. A bifurcation is a place where an artery splits. In figure

3.38 the pressure contour lines are plotted and in figure 3.39 the stream lines. In all cases here $Re_h \approx 6$.

In this case there is only one stenosis in the artery at the right side. The diagonal artery has twice the radius of the horizontal and vertical ones, which have the same the radius. In the picture it is good visible that most of the stream lines take the more easy way out through the normal vessel. As a reference plots are made of the pressure and streamlines in the non-stenotic bifurcation, see figures 3.40 and 3.41. In figures 3.42 and 3.43 the velocity profile just after the bifurcation is plotted in the two directions. In figure 3.42 the profile for the non-stenotic case is plotted. As expected these two profile are exactly the same because the geometry is symmetric.

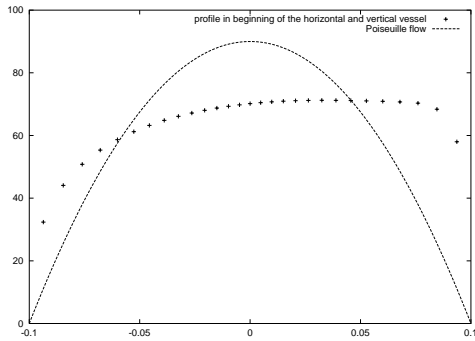


Figure 3.42: Inflow in the after-bifurcation vessel in case of a non-stenotic vessel (dashed) as well as the Poiseuille profile in these cases (line). Dimensions in cm

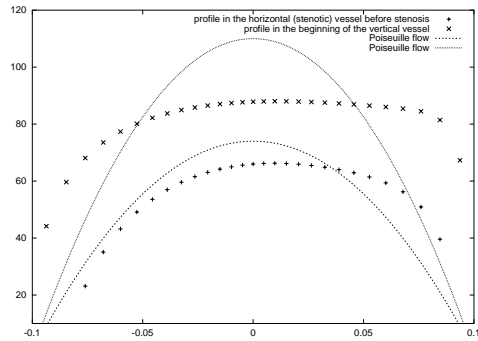


Figure 3.43: Inflow in the after-bifurcation vessel in case of a stenotic vessel (dashed) as well as the Poiseuille profile in these cases (line). Dimensions in cm

In figure 3.43 the same is plotted for the stenotic case. Here the two profile are quite different. The profile just before the stenosis is much lower than the other, which can be expected when we look at the streamlines in this cases. In both cases, however, is this profile not Poiseuille of course because the direction of the flow turns 45° .

3.8 Conclusions

In this chapter we have done the validation of the RNS method and Comflo. As expected are the results nearly the same for large Re_h , but the RNS method calculates much faster. On the other hand, Comflo is better because it can handle almost every geometry, see section 3.7, and has no approximations in his numerical method. Regarding to section 3.6, we can say that there is a effect of a second stenose on the fluid around the first, but this happens only when the second starts immediately after the first and this effect is in fact neglectible small, see figure 3.35.

Chapter 4

The BIACORE 2000

The BIACORE 2000 is used to measure constants or different chemical reactions at the wall of an artery. It consists of some tubes through which a blood-like fluid flows. In this section the fluid through the detection area of the BIACORE 2000 is simulated, especially the wall shear stress at the detection wall. There are a lot of curves in the whole machine, but because the distance between the curves is much larger than the width of the tubes, the fluid after a curve is fully Poiseuille before it arrives at the next curve. The dimensions of the detection unit are given in figure 4.1. At least, these are the dimensions that were given in the Biacore Manual [4]. When the element is observed with a loupe, the height of 2.6 mm can not be right. It should be much smaller. In the simulations we used the real values, given by a Biacore engineer, but it happened to be that the length was still great enough to assume a Poiseuille inflow at each curve.

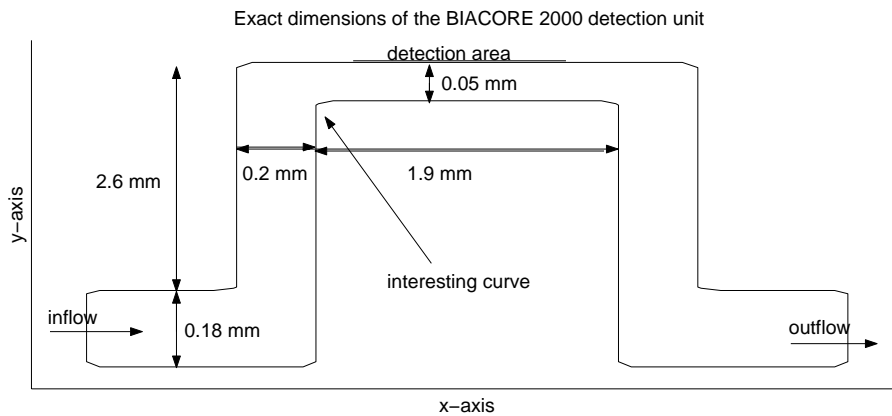


Figure 4.1: The shape of the detection unit in the BIACORE 2000.

In this section only the flow in the neighborhood of the last curve before the detection area is simulated. It is obvious why a Poiseuille inflow is used here. The

pump of the BIACORE 2000 has a range from 5 to 100 $\frac{\mu}{min}$, hence the Reynolds number will vary between 0.55 and 11.

4.1 The flow simulation through the BIACORE 2000

To calculate the exact Poiseuille inflow, different inflow volumes were read from the manual [4] and with them and the dimensions of all parts of the tube a 2D parabolic velocity profile is generated that had the same volume flow as the inlet of the machine. Two dimensional because the simulating is again two dimensional. In figure 4.2 the shape and some stream lines are plotted for the interesting area in the BIACORE 2000.

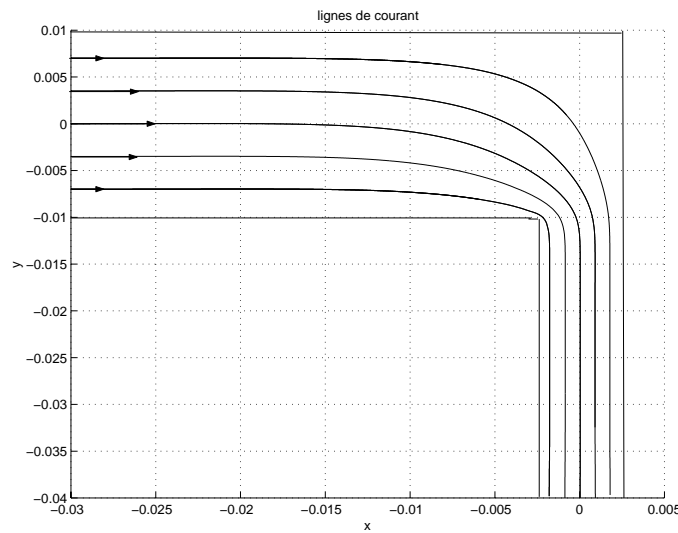


Figure 4.2: The shape, the stream lines and the approximated inflow velocity in the BIACORE 2000.

Because the hospital was especially interested in the wall shear stress at the detection wall, in figure 4.2 $x = 0.0025 \text{ cm}$, plots are made of the wall shear stress between $y = -0.01 \text{ cm}$ and $y = -0.03 \text{ cm}$. After this area the flow is again fully Poiseuille. This can be seen in figure 4.3 at an inflow of 10 $\frac{\mu l}{min}$.

From this picture can be seen that at 0.1 mm after the curve the flow is again Poiseuille. For other values of the inflow volume the shape of the figure stays the same, only the quantity of wall shear stress increases linear. The BIACORE 2000 computes the plaque at the wall only for a small piece of the wall at $x = 0.0025 \text{ cm}$, he assumes the flow to be Poiseuille and starts measuring at a x -value more then 0.1 cm. So the results from the BIACORE 2000 are computed with the correct velocity profile.

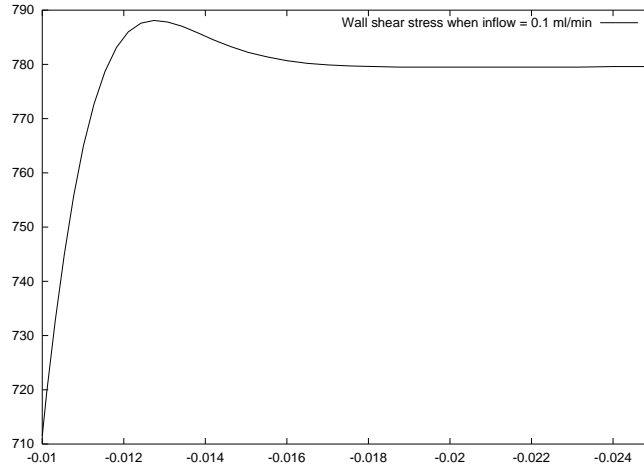


Figure 4.3: The wall shear stress at the wall at $x = 0.0025 \text{ cm}$ with inflow of $100 \frac{\mu\text{l}}{\text{min}}$. ($\text{Re}=0.75$ due to the data from [4].)

4.2 Discussion

$$umax =$$

	11.5	12.0	12.5	13.0	13.5	14.0	14.5	15.0
0.17	135.3	141.1	147.1	152.9	158.8	164.7	170.6	176.5
0.18	127.7	133.3	138.9	144.4	150.0	155.6	161.1	166.7
0.19	121.1	126.3	131.5	136.8	142.1	147.4	152.6	157.9
0.20	115.0	120.0	125.0	130.0	135.0	140.0	145.0	150.0
0.21	109.5	114.3	119.0	123.8	128.6	133.3	138.1	142.9
0.22	104.5	109.1	113.6	118.2	122.7	127.3	131.8	136.4
0.23	100.0	104.3	108.7	113.0	117.4	121.7	126.1	130.4

In the tabular above the absolute wall shear stresses for Poiseuille flow are written for different maximum velocities and different radii. This in case of a Poiseuille flow. The values are determined by computing the analytical solution for $\frac{\partial u}{\partial r}$ where r is the radius of the tube. This results in:

$$\frac{\partial u}{\partial r} = -\frac{2 \text{umax}}{r}$$

The chosen values of $umax$ and r are realistic values of human arteries. The values in the table are for 'healthy' arteries with average radius. The aorta for example has a radius of 0.5 cm , while there exist also narrow arteries with radii much less than 0.1 cm . A wall shear stress of 130 s^{-1} in an arterie with $r_0 = 0.2 \text{ cm}$ will happen at an inflow velocity of $13 \frac{\text{cm}}{\text{s}}$ hence a volume flow of about $17 \frac{\mu\text{l}}{\text{min}}$. The BIACORE 2000 has a pump range of $5\text{-}100 \frac{\mu\text{l}}{\text{min}}$. Hence the wall shear stress varies between 39 and 780 s^{-1} . So the realistic human artery values are among them. So the maximum

wall shear stress that can be reached by the BIACORE 2000 is 780 s^{-1} . This does not include all the wall shear stresses of stenotic vessels. In the worst case, with a very narrow stenosis, wall shear stresses have been measured to be around 20000 s^{-1} .

When a pulsatile inflow is used, a Womersley profile will develop after a long enough distance in the tube. An important quantity here is $\alpha = r_0^2 \frac{\omega}{\nu}$. In figure 4.4 the wall shear stress is plotted for three values of α using Mathematica. The points are the values for $\alpha = 1$, the line is for $\alpha = 10$ and the upper values are for $\alpha = 50$. From this picture it is not strange to suggest that the maximum value of the wall shear stress is equal to $\sqrt{\alpha}$, which should hold for large α , see Appendix A. At least for the $\alpha = 50$ it seems to hold ($\sqrt{50} \approx 7.07$).

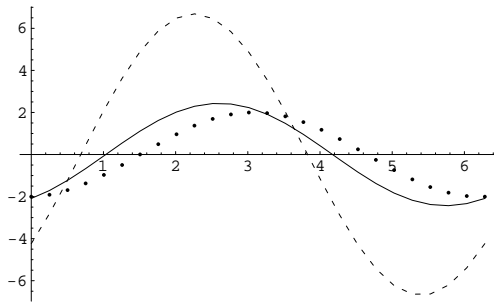


Figure 4.4: For $\alpha = 1, 10,$ and 50 the wall shear stress is plotted as function of time for one period.

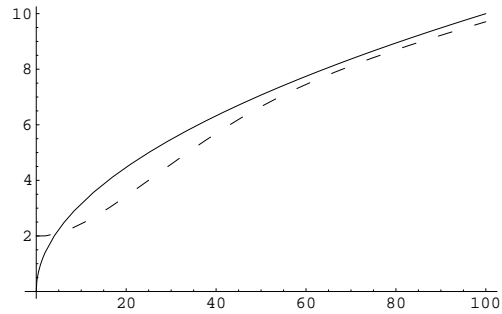


Figure 4.5: The dashed line is the maximal wall shear stress as function of α . The other is the asymptotic value $\sqrt{\alpha}$.

So in figure 4.5 the maximum wall shear stress as function of α is plotted as well as the curve $y = \sqrt{\alpha}$. Now it is clearly visible that for large value of α the maximum wall shear stress is nearly $\sqrt{\alpha}$. Anyway for all α the wall shear stress is of the order of $\sqrt{\alpha}$. At last some typical values for different arteries are presented here.

artery	diameter	α
Ascending aorta	1.5 <i>cm</i>	174.2
Descending aorta	1.3 <i>cm</i>	132.3
Femoral Artery	0.4 <i>cm</i>	12.3
Carotid artery	0.5 <i>cm</i>	19.4

Chapter 5

Three dimensional stenosis flow

In this chapter the program COMFLO, see Kort [8] and Loots [12], is used to simulate 3D flow blood through a stenosis in an artery. Therefore a cylindrical geometry is used which was already implemented in COMFLO. The z -axis will be used here as the length of the artery.

The stenosis can be defined in two ways. In the first case a stenosis only in the x -direction is used, letting the radius of the y -direction constant. This is visualized in figure 5.1. This problem is more similar to the 2D-problem than the second, but the latter is more realistic.

The second stenosis is an axisymmetrical stenosis. This geometry is plotted in figure 5.4.

5.1 'One direction' stenosis

In this section the results from the 2D geometry in section 3.2, now with constant inflow will be compared with the results from the geometry in figure 5.1.

The inflow velocity is taken equal to 1 in both cases. The velocity profile in the middle of the artery is shown in 5.2. The pressure profile is shown in figure 5.3.

In the picture of the velocities, the velocity of the 3D flow is higher than the 2D flow. The most important thing in explaining this occurrence is that COMFLO uses, when he simulates a 2D flow, a 3D geometry in which the z -direction has only one cell. Whatever the dimensions are, the 2D geometry will always be extended in the z -direction. So in the used 2D cases, the geometry is a beam.

At two walls, $y = y_{max}$ and $y = y_{min}$, the velocity is taken 0, but at the other two (in z -direction) not. The velocity profile in the tube will be Poiseuille as seen in figure 3.4. So this 2D velocity profile is only 0 at $y = y_{min}$ and $y = y_{max}$, not at z_{min} and z_{max} .

This profile is of the form:

$$u(x) = 1.5u_{in} \left(1 - \frac{x^2}{h^2} \right)$$

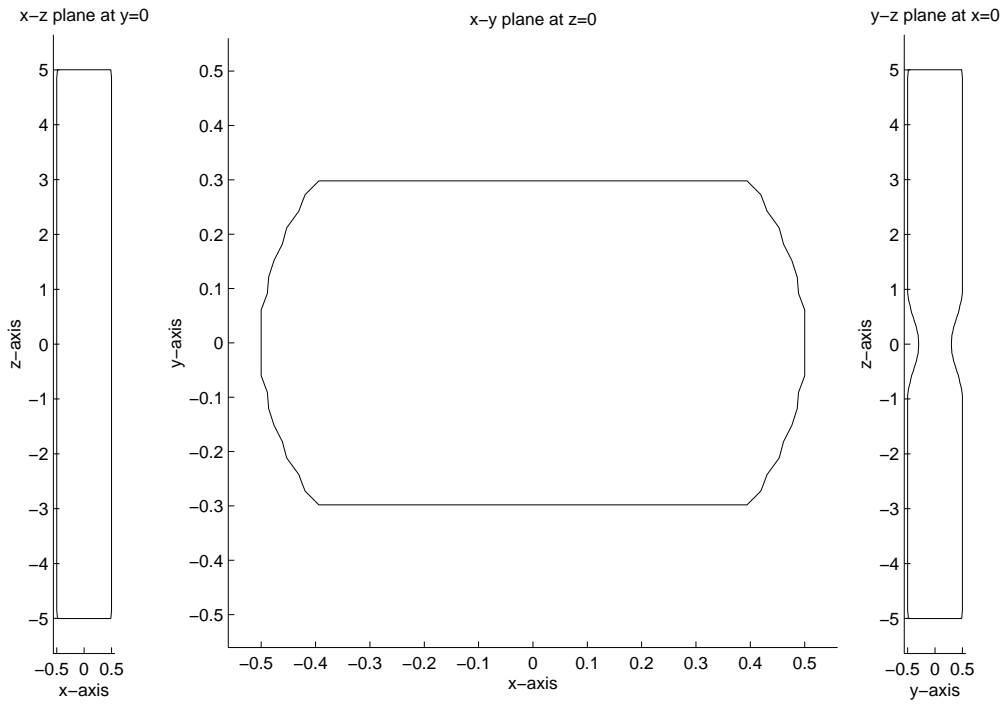


Figure 5.1: The different planes of the geometry for a 'one direction' stenosis.

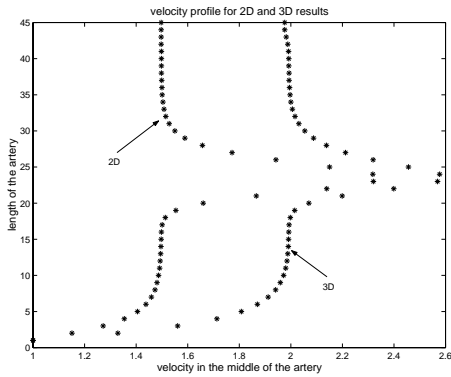


Figure 5.2: Velocity profiles

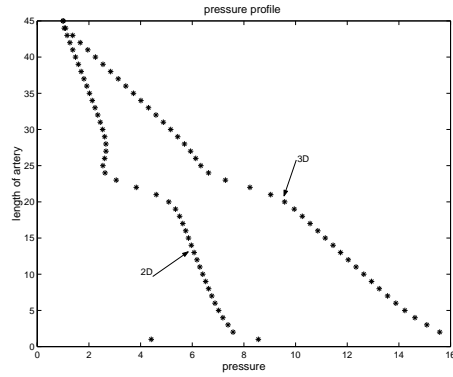


Figure 5.3: Pressure profiles

because

$$\frac{1}{h} \int_0^h u(x) dx = u_{in}$$

In the 3D case the velocity at the wall of the whole cylinder is taken to be 0 so we get a 3D Poiseuille velocity profile. This profile has to have a higher maximum to get the same average value which should be equal to u_{in} . The 3D velocity profile is

of the form :

$$u(x, y) = 2u_{in}\left(1 - \frac{1}{h^2}(x^2 + y^2)\right)$$

because

$$\frac{1}{\pi h^2} \int \int_{x^2+y^2=h^2} u(x) dx dy = u_{in}$$

In the first case, the maximum is equal to $1.5u_{in}$. This is smaller than $2u_{in}$ from the second case. So the velocity in a straight tube will always be higher if a 3D axisymmetrical geometry is used instead of a 2D geometry. These values are good visible in the pictures.

5.2 Axisymmetrical stenosis

In this section blood flow through the geometry shown in figure 5.4 will be discussed. This situation is more realistic in the case of blood vessel flow. In this 3D case with

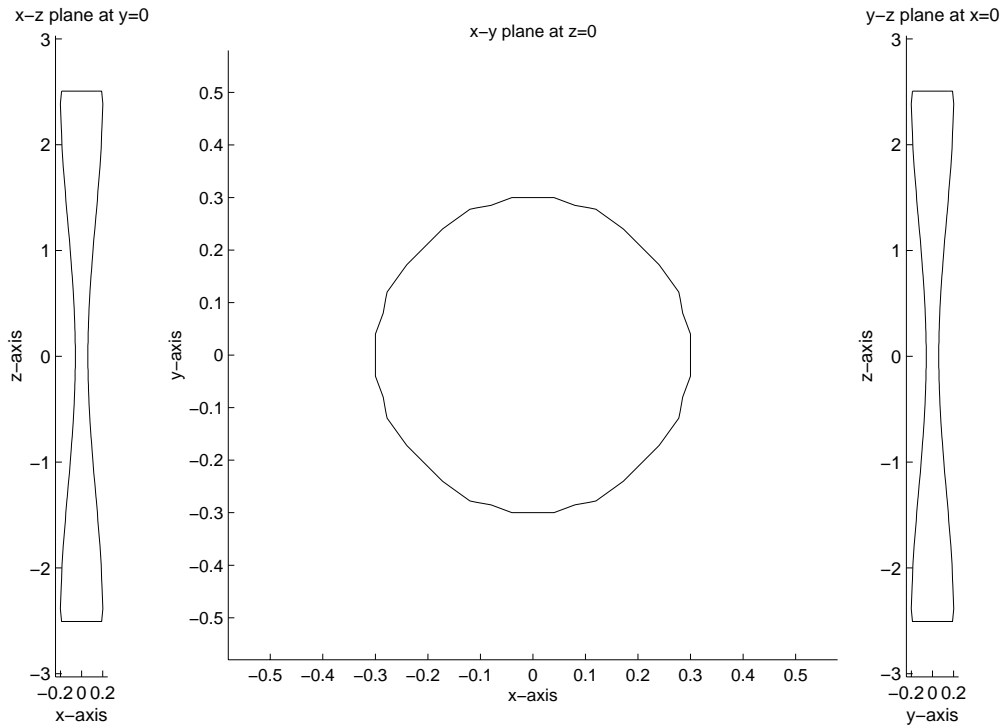


Figure 5.4: The different planes of the geometry for an axisymmetrical stenosis.

an axisymmetrical geometry we used again only time-independent inflow because it takes a lot of time for Comflo to calculate a 3D flow, especially when the inflow is dependent of time. With the chosen inflow we always have a stationary solution after some time. Three different kinds of inflow are chosen:

1. $u(x, y, t) = u_{in} = cst$ flat inflow
2. $u(x, y, t) = 2u_{in}(1 - \frac{1}{h^2}(x^2 + y^2))$ Poiseuille inflow
3. $u(x, y, t) = a + bx$. With a and b chosen so that the volume flow in the three cases stays the same. We will call this the 'scheef' inflow.

We choose different inflows because we want to know what the influence if of the entry profile at the final flow. These profiles are chosen because the first two are simple profile in 3D and the third inflow is a approximations of the inflo in a stenosis that is located just after a bifurcation, like in figure 3.38 and 3.39. In figure 5.5 these different velocities are plotted at the x-axis for $y=0$. In each of the three cases a total inflow of $240 \frac{ml}{min}$ is taken. This results in a Re_h of 600.

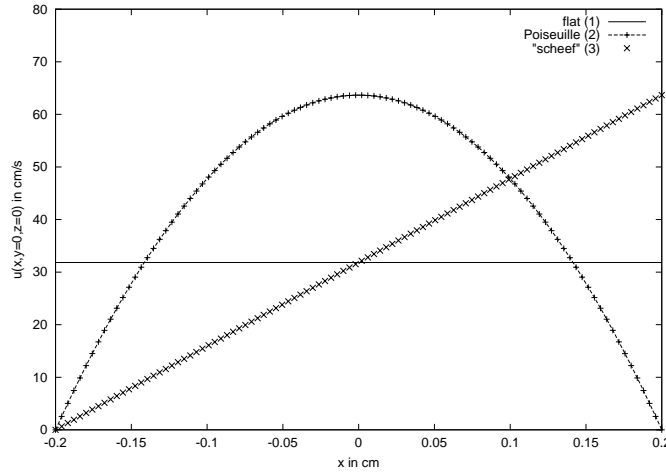


Figure 5.5: The three different inflow of this section. Dimensions in cm

In figure 5.6 the velocities in the middle of the tube in the three different cases of inflow are plotted. Of course the Poiseuille inflow starts with a higher velocity but will come closer to the other two. In this case 30 points in x- and y-direction are used and 60 in z-direction. This is not very much and that is why more points are used in the further examples. In figure 5.7 the same is plotted with a 50X50X100 grid. These results are different but with the example with a 50X100X100 grid the calculation of Comflo takes about 5 days on a Linux PC 750 instead of less than an hour for a 30X30X60 grid!

In figures 5.8, 5.9 and 5.10 the velocity in the middle of the tube is plotted for the case of all different inflows for different numbers of points. Now it is clear that it is very important that enough points are used, especially for the area after the stenosis. The examples with the finest grid looks most like the RNS results. This can be seen in figure 5.11. Here the velocities in the middle of the tube made by Comflo and by the RNS method are plotted. The RNS method in this section uses only a flat profile.

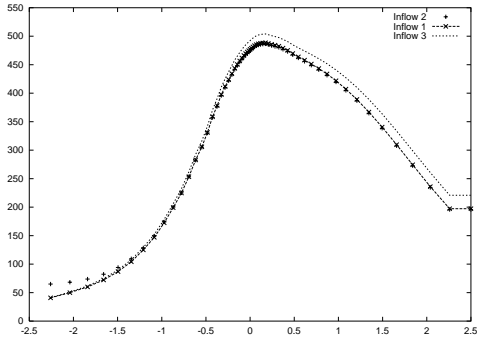


Figure 5.6: The velocities for Comflo with the three different inflows. 30X30X60 points in stretched grid. Dimensions in *cm*

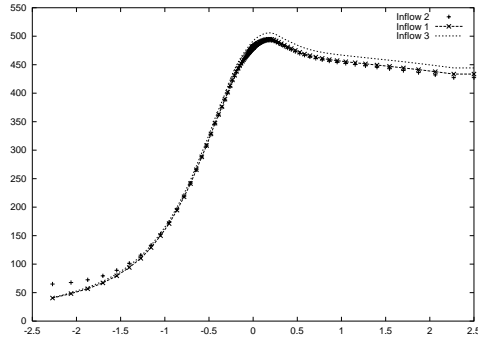


Figure 5.7: The velocities for Comflo with the three different inflows. 50X50X100 points in stretched grid. Dimensions in *cm*

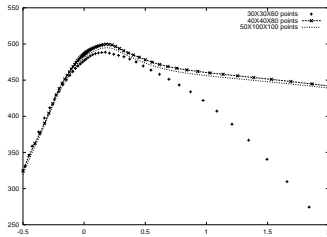


Figure 5.8: The velocities in the middle of the tube in case of a flat inflow(1). Different numbers of points are used. Dimensions in *cm*

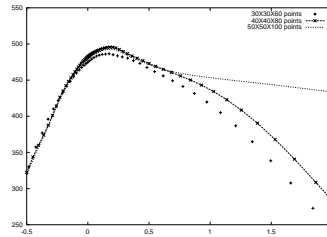


Figure 5.9: The velocities in the middle of the tube in case of a Poiseuille inflow(2). Different numbers of points are used. Dimensions in *cm*

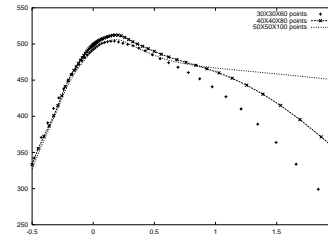


Figure 5.10: The velocities in the middle of the tube in case of a 'scheef' inflow(3). Different numbers of points are used. Dimensions in *cm*

To get an idea of the flow in transversal direction through such a axisymmetrical stenosis, there are 9 plots made using arrows to indicate the direction of the flow in the $x-y$ plane. Three plots for every type of inflow respectively in the beginning of the stenosis, in the middle and just before the end. This can be seen in figure 5.12, 5.13, 5.14. Note that the picture for the middle of the stenosis have the same size so of course another x and y -scale is used than in the first and the third. That is why there are less arrows in the picture (less points).

When we take a first look at the picture, the picture for the end of the stenosis for inflow 2 and 3 are not symmetric. We expected this any way for the inflow 2, Poiseuille, because an axisymmetrical inflow through an axisymmetric tube with an axisymmetrical stenosis would expect an axisymmetrical outflow. Then we notice that even in the beginning of the stenosis the Poiseuille flow is not axisymmetric anymore. This requires an explanation.

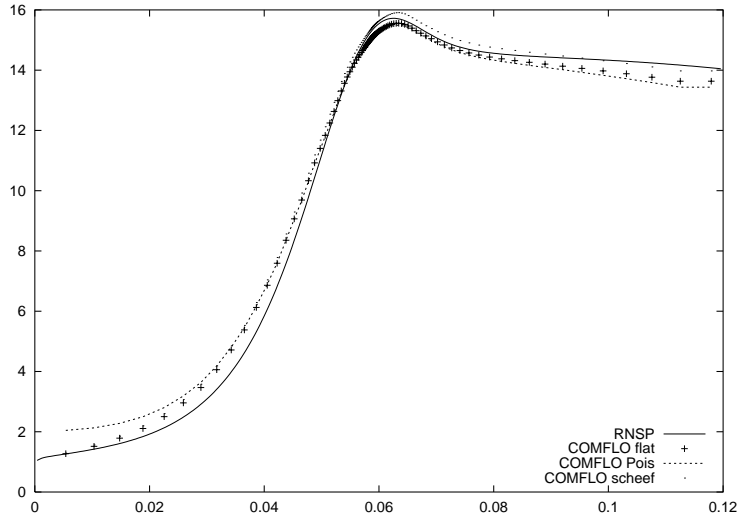


Figure 5.11: The velocities in the middle for Comflo and RNS. Comflo uses here 50X50X100 points. Dimensionless scales!

Because only the direction is given for the transversal velocity, it says nothing about the actual speed. When we look better at all the data, it happens that the longitudinal flow is $O(10^1)$ in the beginning of the tube, the three figures on the left, and of $O(10^2)$ in the stenose and at the end of the tube, see also figure 5.6 and 5.7. The transversal velocity, on the contrary, is in the middle and at the end of tube of order 10^{-2} , so in the 6 pictures most at the right. Because there is such a large difference between these orders, we can say that the unexpected details of the figures are just errors of the calculations.

In the beginning of the tube, the left three figures, the order of the transversal velocities in case of Poiseuille inflow (2) is also 10^{-2} and of the other two is 10^0 so that even the first image of 5.13 can be neglected. As a result, only the first picture of figure 5.12 and 5.14 are valuable for us.

Because 5.12 has an inflow that is constant for both x and y , so the fluid will go simultaneously to the center of the tube when we proceed in the tube. In figure 5.14 the inflow 3 is used, which is high for high values of x and 0 at the lower boundary of x . So this picture makes sense because the velocity is negative in the x -direction for $x > -0.1$ and is much larger than in positive x -direction for $x < -0.1$. All the fluid has to go to the center of the tube and at the right-hand side there a lot enters the tube because of the inflow condition!

So the influence of the exact inflow profile is very weak: a 3D profile can not be recognized after the stenosis. It's changed into a nearly axisymmetrical one!

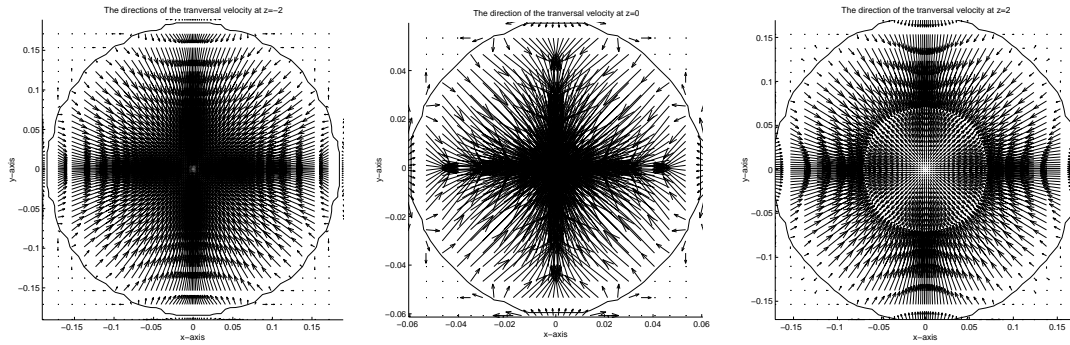


Figure 5.12: Transversal velocity directions for a flat inflow (1). Resp. begin, middle and end of stenosis

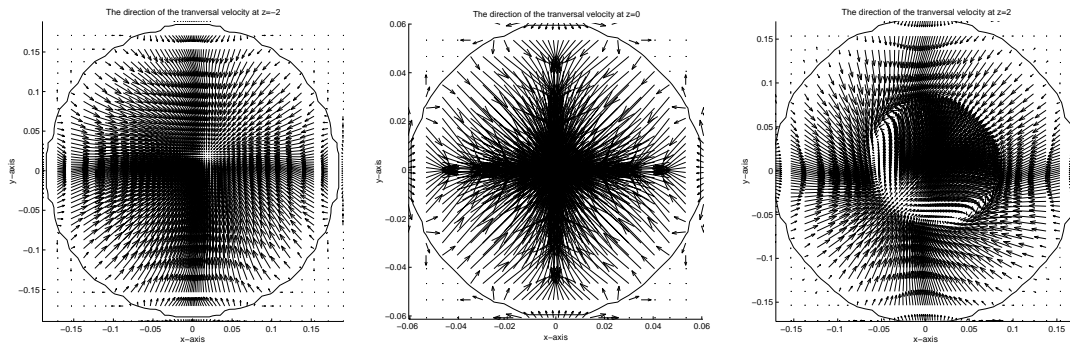


Figure 5.13: Transversal velocity directions for Poiseuille inflow (2). Resp. begin, middle and end of stenosis

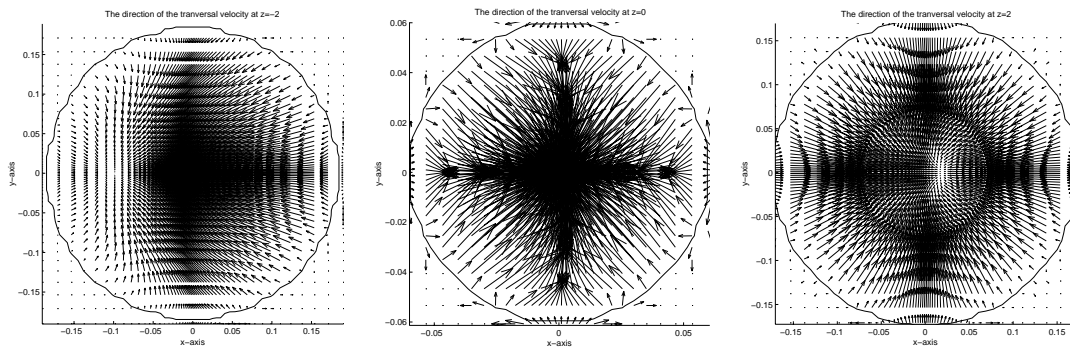


Figure 5.14: Transversal velocity directions for 'scheef' inflow (3). Resp. begin, middle and end of stenosis

Chapter 6

Conclusions

In the last 100 days there are made a lot of simulation of arteries with stenoses. Most of the different cases for a straight artery are handled, 2D as well as 3D. The RNS method of the university here in Paris is validated and shows in most cases really good results for large Re_h in comparison with the complete NS-solver COMFLO. This is not strange because in the RNS method a large Re_h is supposed, see section 2.3. In examples with constant inflow, the results are almost the same. For pulsatile inflow, the results for the pressure is different between COMFLO and RNS, especially in the accelerarating and decelerating phase, see figure 3.11 and 3.13.

We have focused in this study on the entry effect on the flow further in and after the stenosis and we have observed that in most cases the first profile is very important. See figures 5.11 for Poiseuille, flat and 'scheef' profile in a axisymmetrical case.

Although we are a step closer to really simulate blood flow through human arteries, a lot has still to be done. The geometries that are used are still straight, stiff tubes. Most of the simulations are done for the 2D case because COMFLO needs a lot of time to handle 3D flows. In real world, only 3D simulations of curved tubes with an elastic wall are realistic blood vessels. See Berger [2] for examples of stenosis with realistic dimensions and properties. Further, real human arteries have almost never a smooth wall nor are axi-symmetrical. COMFLO is able to simulate flow through 3D tubes with another radius in y -direction then in x -direction, but such an ellipsis is still a large approximation.

Simulating flows through objects which are designed by nature, such as arteries, is so complicated that we might never be able to do that with high detailed geometries and high precision results. However, flows through machines that are related to blood flows and make their own measurements on it, like the Biacore 2000, are also approximations of the real world and can be very good simulated by COMFLO as we have seen in Chapter 4.1.

Appendix A

Womersley analysis

A.1 The direct Womersley solution

If a pulsatile inflow is used in a straight rigid tube, the velocity after a long enough distance will have a Womersley profile. This profile can be derived from the dimensionless axisymmetrical conservation of momentum:

$$\frac{\partial u}{\partial t} = -\frac{1}{\rho} \frac{\partial p}{\partial x} + \nu \left(\frac{\partial^2 u}{\partial x^2} + \frac{1}{r} \frac{\partial u}{\partial r} + \frac{\partial^2 u}{\partial r^2} \right) \quad (\text{A.1})$$

Where ν is the viscosity of the fluid. We suppose every variable to be proportional to $e^{i\omega(t-\frac{x}{c})}$, where c is the complex wave speed and ω the frequency, so $\lambda = 2\pi\frac{c}{\omega}$. We simplify the equation by making the long-wavelength approximations $|\frac{\omega R}{c}| \ll 1$, where R is the radius of the tube. The $\frac{\partial^2}{\partial x^2}$ -term is now negligible because it is of order λ^{-2} . So when we suppose

$$u = e^{i\omega t} \hat{u} \quad \text{and} \quad p = e^{i\omega t} \hat{p}$$

the equation will reduce to:

$$-\frac{i\omega}{\nu} \hat{u} + \frac{1}{r} \frac{\partial \hat{u}}{\partial r} + \frac{\partial^2 \hat{u}}{\partial r^2} = \frac{1}{\nu \rho} \frac{\partial \hat{p}}{\partial x} \quad (\text{A.2})$$

When we introduce $y = \frac{r}{K}$, the equation will convert to:

$$-\frac{i\omega}{\nu} \hat{u} + \left(\frac{1}{y} \frac{\partial \hat{u}}{\partial y} + \frac{\partial^2 \hat{u}}{\partial y^2} \right) \frac{1}{K^2} = \frac{1}{\mu} \frac{\partial \hat{p}}{\partial x}$$

If we choose $K = \sqrt{\frac{\nu}{-i\omega}}$ we derive an equation that looks like the Bessel equation:

$$\frac{\partial^2 \hat{u}}{\partial y^2} + \frac{1}{y} \frac{\partial \hat{u}}{\partial y} + u = \frac{1}{\mu} \frac{\partial \hat{p}}{\partial x} K^2 \quad (\text{A.3})$$

The solution of this equation is the sum of an particular solution and the exact solution from the homogene equation, which is the Bessel equation (Remember that

the solution of $f'' + f'/x + f(x^2 - n^2)/x^2 = 0$ is $J_{\pm n}$ and $Y_{\pm n}$, see Abramowitz and Stegun [1]). The first solution is $u = cst = \frac{1}{\mu} \frac{\partial \hat{p}}{\partial x} K^2$. The second is Bessel function $A J_0(y)$. So the total solution will be:

$$\hat{u}(y) = A J_0(y) + \frac{1}{\mu} \frac{\partial \hat{p}}{\partial x} \frac{\nu}{-i\omega} \quad (\text{A.4})$$

with boundary condition

$$\hat{u}(r = R) = 0$$

Because $\hat{u}(y) = \hat{u}(\frac{r}{R})$, filling in the boundary condition will lead to:

$$0 = A \left(J_0 \left(i^{\frac{3}{2}} R \sqrt{\frac{\omega}{\nu}} \right) \right) + \frac{1}{\mu} \frac{\partial \hat{p}}{\partial x} \frac{\nu}{-i\omega} \Rightarrow A = \frac{-\frac{1}{\mu} \frac{\partial \hat{p}}{\partial x} \frac{\nu}{-i\omega}}{J_0 \left(i^{\frac{3}{2}} R \sqrt{\frac{\omega}{\nu}} \right)}$$

So the final solution for $U_{wom}(r, t) = \hat{u}e^{i\omega t}$ is:

$$U_{wom}(r, t) = e^{i\omega t} \frac{1}{\rho} \frac{\partial \hat{p}}{\partial x} \frac{1}{-i\omega} \left(1 - \frac{J_0 \left(i^{\frac{3}{2}} \frac{r}{R} \sqrt{\alpha} \right)}{J_0 \left(i^{\frac{3}{2}} \sqrt{\alpha} \right)} \right) \quad \text{with} \quad \alpha = R^2 \frac{\omega}{\nu} \quad (\text{A.5})$$

A.1.1 Plots of U_{wom}

In this subsection plots are made of $\Re(U_{wom})$ and $\Im(U_{wom})$ for different values of α . In each plot to velocity profile between $\tilde{y} = 0$ and 1 is given for four different times: $t = 0, 2\frac{\pi}{5}, 4\frac{\pi}{5}, 6\frac{\pi}{5}$.

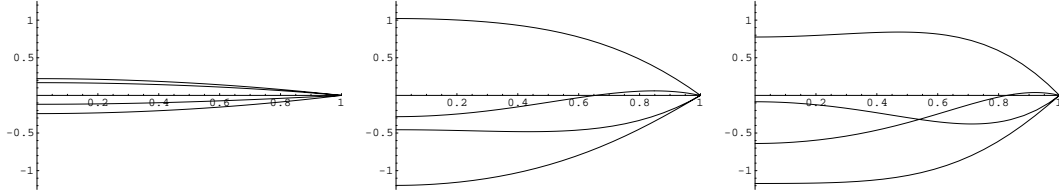


Figure A.1: $\Re(U_{wom})$. From left to right $\alpha = 1, 10, 20$.

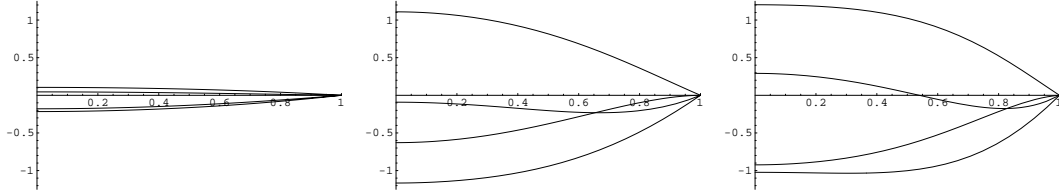


Figure A.2: $\Im(U_{wom})$. From left to right $\alpha = 1, 10, 20$.

Notice that the velocity in the middle for larger α don't change anymore, while the first derivative is bigger for larger α near the wall.

A.1.2 Putting α large in the solution

According to Abramowitz [1], for a large z , the BesselFunction $J_k(z)$ will become:

$$\text{As } z \rightarrow \infty \quad J_k(z) \sim \sqrt{\frac{2}{\pi z}} \left(\cos\left(z - \frac{k\pi}{2} - \frac{\pi}{4}\right) + O\left(\frac{1}{|z|}\right) \right)$$

When we substitute for $z = i^{\frac{3}{2}}y$, $k = 0$ and use the known equalities:

$$\sqrt{i} = \frac{i+1}{\sqrt{2}} \quad \text{and} \quad \cos(t) = \frac{1}{2}(e^{it} + e^{-it}) \quad (\text{A.6})$$

We obtain the equation from Pedley [14] for the BesselFunction $J_0(z)$ for large y :

$$J_0(i^{\frac{3}{2}}y) \sim \frac{e^{\frac{y}{\sqrt{2}}}}{\sqrt{2\pi y}} e^{i\left(\frac{y}{\sqrt{2}} - \frac{\pi}{8}\right)} \left(1 + O\left(\frac{1}{y}\right)\right)$$

With this function for J_0 , U_{wom} can be written as:

$$U_{wom}(r, t) = U_{wom}(0, t) \left(1 - e^{-\sqrt{\frac{\alpha}{2}}(1+i)\left(1 - \frac{r}{R}\right)}\right) \quad (\text{A.7})$$

When $\alpha \rightarrow \infty$ and $r < R$ it is clear that $U_{wom}(r, t) = U_{wom}(0, t)$, so independent of position from the wall. But when $r \rightarrow R$ as $\frac{1}{\sqrt{\alpha}}$ the value of the exponential is of order one and so we see there is a boundary layer of thickness $\frac{1}{\sqrt{\alpha}}$ in which the velocity goes from $U_{wom}(0, t)$ to 0.

A.2 Asymptotical point of view α large

A.2.1 Perfect fluid

We look at the same problem, but with the point of view of asymptotic analysis. First we adimensionalise the equations:

$$\hat{u} = \frac{1}{\rho\omega} \frac{\partial p}{\partial x} \bar{u} \quad \text{and} \quad r = \bar{r}R$$

Equation A.2 will now become:

$$-i\bar{u} + \frac{1}{\alpha} \left(\frac{1}{\bar{r}} \frac{\partial \bar{u}}{\partial \bar{r}} + \frac{\partial^2 \bar{u}}{\partial \bar{r}^2} \right) = 1 \quad (\text{A.8})$$

If $\alpha \rightarrow \infty$, we obtain the "Euler" problem (or perfect fluid). The velocity is constant all over the radius: $\bar{u} = i$. The no slip condition is not full fit. We have to introduce a boundary layer of unknown thickness ε in order to have the good boundary condition. The idea is to change the transversal scale because the viscosity acts in a very thin layer near the wall. In this layer we want to have the viscous terms that were neglected before.

A.2.2 Boundary layer

Close to the wall the following changement of variables is made for r and \hat{u} in A.2.

$$r = R(1 - \varepsilon\tilde{y}) \quad \varepsilon \ll 1 \quad \text{and} \quad \hat{u} = \frac{1}{\rho\omega} \frac{\partial p}{\partial x} \tilde{u} \quad (\text{A.9})$$

It can be done because $\frac{\partial p}{\partial x}$ is independent of the y or r -direction. With this change-ment the $\frac{\partial u}{\partial r}$ -term in A.2 vanishes because it is of order ε . The equation will then become:

$$-iu + \frac{1}{\alpha} \left(\frac{1}{\varepsilon^2} \frac{\partial^2 u}{\partial \tilde{y}^2} + O(\varepsilon^{-1}) \right) = 1$$

Again we look at the case of large α : because here by the choice of scale $\frac{\partial^2 u}{\partial \tilde{y}^2} \sim O(1)$ we have to make sure that $\frac{1}{\alpha} \frac{1}{\varepsilon^2} \sim O(1)$ so we choose $\alpha\varepsilon^2 = 1 \Rightarrow \varepsilon = \sqrt{\frac{1}{\alpha}}$. The thickness of the boundary layer is then $\alpha^{-1/2}$. The equation is now:

$$-i\tilde{u} + \frac{\partial^2 u}{\partial \tilde{y}^2} = 1$$

with only order one coefficients. There are two possible solutions: $\tilde{u} = A(1 - e^{-\tilde{y}\sqrt{i}})$ and $\tilde{u} = A(1 - e^{\tilde{y}\sqrt{i}})$, with A un up to now undetermined constant. From these two we obviously choose the first one because the last one will tend to $-\infty$ for $y \rightarrow \infty$. Notice that $\tilde{u}(0) = 0$ in both cases! That is what we wanted: the no-slip condition. In order to determine A we have to match the perfect fluid layer and the boundary layer:

$$\bar{u}(\bar{r} \rightarrow 1^-) = \tilde{u}(\tilde{y} \rightarrow \infty)$$

so the final solution is:

$$A = i \quad \implies \quad \tilde{u} = i(1 - e^{-\tilde{y}\sqrt{i}}) \quad (\text{A.10})$$

A.3 Remarks

In general, the fluid mech. problems have no analytical solution. Here we have one, and we observe that the asymptotic solution, A.10, is the analytical one, A.7, when $\alpha \rightarrow \infty$. When you substitute $\tilde{y} = \frac{1}{\varepsilon}(1 - \frac{r}{R}) = \sqrt{\alpha}(1 - \frac{r}{R})$ and $\hat{u} = \frac{1}{\rho\omega} \frac{\partial p}{\partial x} \tilde{u}$ in A.10, we find the solution A.7 because $J_0(i^{\frac{3}{2}}\sqrt{\alpha}) \rightarrow \infty$ for $\alpha \rightarrow \infty$, so $U_{wom}(0, t) = e^{i\omega t} i$

A.3.1 The wall shear stress

If $y \rightarrow 0$, because

$$\frac{\partial u}{\partial r} = \frac{1}{\varepsilon} \frac{\partial u}{\partial \tilde{y}} = \sqrt{\alpha} \frac{\partial u}{\partial \tilde{y}} \quad \text{and} \quad \frac{\partial u}{\partial \tilde{y}} = O(1)$$

We can conclude that the wall shear stress $\frac{\partial u}{\partial r} \approx \sqrt{\alpha}$.

A.4 Small α

A.4.1 Analytical solution for small α

The analytical solution U_{wom} from A.5 can we write as:

$$U_{wom}(r, t) = f(t) \left(1 - \frac{J_0(i^{\frac{3}{2}} \frac{r}{R} \sqrt{\alpha})}{J_0(i^{\frac{3}{2}} \sqrt{\alpha})} \right)$$

If $z \rightarrow 0$, Pedley [14] says that $J_0(z) \sim 1 - \frac{1}{4}z^2$. So if $\alpha \rightarrow 0$ we can write U_{wom} as:

$$\begin{aligned} U_{wom}(r, t) &= f(t) \left(1 - \frac{1 + \frac{i}{4} \frac{r^2}{R^2} \alpha}{1 + \frac{i}{4} \alpha} \right) \\ &\quad \Downarrow \\ U_{wom}(r, t) &= f(t) \frac{-i\alpha}{4 + i\alpha} \left(1 - \frac{r^2}{R^2} \right) \end{aligned} \quad (\text{A.11})$$

which has a parabolic form and is 0 for $r = R$ at a fixed time. So here we refind the Poiseuille profile. This is not strange because $\alpha = 0$ implies $\omega = 0$ because both R and $\nu \in \mathbb{R}^+$. ω was the frequency, and frequency of 0 means an infinit long period thus a constant (i.e. time-independent) flow. Notice that the amplitude is also small for small α as we have already seen in figures A.1 and A.2.

A.4.2 Asymptotic solution for small α

With α as in A.5 we can write equation A.2 as :

$$-\frac{i\alpha}{R^2}u + \frac{1}{r} \frac{\partial u}{\partial r} + \frac{\partial^2 u}{\partial r^2} = \frac{1}{\mu} \frac{\partial p}{\partial x} \quad \text{with} \quad \mu = \rho\nu$$

As in section A.2.1 we adimensionalize the equations using:

$$u = \frac{R^2}{\mu} \frac{\partial p}{\partial x} \bar{u} \quad \text{and} \quad r = \bar{r}R$$

This results in:

$$-i\alpha \bar{u} + \frac{1}{\bar{r}} \frac{\partial \bar{u}}{\partial \bar{r}} + \frac{\partial^2 \bar{u}}{\partial \bar{r}^2} = 1$$

The first term will disappear when we let $\alpha \rightarrow 0$, so we get:

$$\frac{1}{\bar{r}} \frac{\partial \bar{u}}{\partial \bar{r}} + \frac{\partial^2 \bar{u}}{\partial \bar{r}^2} = 1 \quad \implies \quad \bar{u} = -\frac{1 - \bar{r}^2}{4}$$

This solution is again a Poiseuille flow.

Appendix B

Explanatory vocabulary

accelerating phase	time range in which a pulse goes to higher velocities
aneurysm	widhtening of an artery
bifurcation	an artery that splits in two smaller arteries
boundary layer	a very thin layer between an object and the fluid in which the longitudinal velocity will vary from 0 at the object wall to the outer velocity at the other side of the layer
carotid artery	the main artery that is going to the head
COMFLO	program designed in Groningen that solves the complete NS-equations
decelerating phase	time range in which a pulse goes to lower velocities
discretization	way of approximating a continuous problem with a discrete problem
femoral artery	the main artery that is going to the leg, so there are two of them
longitudinal velocity	velocity in the direction of the length of the tube
iteration	(repetition of a) calculation
iteration process	process with repeated calculations
NS	method designed in Groningen that solves the Navier-Stokes equations numerically <i>or</i> the equations on which this method is based
RNS / RNSP	method desinged in Paris that solves the Reduced Navier-Stokes equations numerically <i>or</i> the equations on which this method is based
RuG	University of Groningen; <i>Dutch</i> : Rijksuniversiteit Groningen
stenosis	narrowing or stricture of an artery
transversal velocity	velocity in the cross-section of an artery

Bibliography

- [1] M. Abramowitz, I. A. Stegun (1970): “Handbook of Mathematical Functions” Dover publications, Inc., New York.
- [2] S. A. Berger, L-D. Jou (2000): “Flows in Stenotic Vessels” *Annu. Rev. Fluid Mech.* 2000. 32:347:382
- [3] D. Bluestein, L. Niu, R. T. Schoephoerster, M. K. Dewanjee (1996): “Steady Flow in an Aneurysm Model: Correlation Between Fluid Dynamics and Blood Platelet Deposition” *Journal of Biochemical Engineering*, august 1996 p 280-286
- [4] “BIACORE 2000 Instrument Handbook”: Chapter 2 and Appendix A
- [5] R. Budwig, D. Elger, H. Hooper, J. Slippy (1993): “Steady Flow in Abdominal Aortic Aneurysm Models”. *Journal of Biochemical Engineering*, november 1993 p 418-423.
- [6] R. Comolet (1982): “*Mécanique Expérimentale des Fluides.*” Masson, Paris.
- [7] Koen Goorman (2000): “Steady and unsteady channel flows, numerical models with applications to the recorder flute and vocal folds modeling”. Master’s Thesis TU Eindhoven
- [8] Dirk-Jan Kort (2000): “Numerical Simulations of the blood flow in the arteria carotis communis: a pilot study”. Report *RuG*
- [9] P.-Y. Lagrée (2000): “An inverse technique to deduce the elasticity of a large artery.”
- [10] P.-Y. Lagrée & S. Lorthois (1999): “Interacting Boundary layer flow in a stenosis”. *Archives of Physiology and Biochemistry* Vol 107 sept 99, p 51.
- [11] P.-Y. Lagrée & M. Rossi (1997): “Modélisation de l’écoulement sanguin par une approche de type couche limite instationnaire. Mise en oeuvre d’une méthode inverse pour trouver l’élasticité de la paroi et la viscosité du fluide.”
- [12] Erwin Loots (1998) “Free Surface Flow in 3D Complex Geometries using Enhanced Boundary Treatment”. Master’s Thesis *RuG*

- [13] Lorthois S. & Lagrée P-Y (2000): “Écoulement dans un convergent axisymétrique: calcul de la contrainte de cisaillement parital maximale/ Flow in a axisymmetric convergent: evaluation of maximum wall shear stress”, C. R. Acad. Sci. Paris, t328, Srie II b, p33-40, 2000
- [14] Pedley T.J. (1980): “The fluid mechanics of large blood vessels”, Cambridge University press.
- [15] H. Schlichting (1987): “Boundary layer theory” 7th ed Mc Graww Hill.
- [16] Siegel, J.M Markou, C.P. Ku, D.N. and Hanson, S.R (1994): “A scaling law for wall shear stress through an arterial stenosis”, ASME Journal of Biomechanical Engineering 116, 446- 451.
- [17] Veldman, A.E.P. “Grenslaagstromingen” Lecture notes RuG
- [18] Young, D.F. (1979):“Fluid Mechanics of Arterial Stenoses”. ASME Journal of Biomechanical Engineering 101, 157- 173.